

MASSIVE SCHWINGER MODEL WITHIN MASS PERTURBATION THEORY*

Christoph Adam[†]

*Center for Theoretical Physics
Laboratory for Nuclear Science
and Department of Physics
Massachusetts Institute of Technology
Cambridge, Massachusetts 02139
and
Inst. f. theoret. Physik d. Uni Wien
Boltzmannngasse 5, 1090 Wien, Austria*

(MIT-CTP-2618, March 1997)

Abstract

In this article we give a detailed discussion of the mass perturbation theory of the massive Schwinger model. After discussing some general features and briefly reviewing the exact solution of the massless case, we compute the vacuum energy density of the massive model and some related quantities. We derive the Feynman rules of mass perturbation theory and discuss the exact n -point functions with the help of the Dyson-Schwinger equations. Further we identify the stable and unstable bound states of the theory and compute some bound-state masses and decay widths. Finally we discuss scattering processes, where the resonances and particle production thresholds of the model are properly taken into account by our methods.

Typeset using REVTeX

[†]Email address: adam@ctp.mit.edu, adam@pap.univie.ac.at

*This work is supported by a Schrödinger Stipendium of the Austrian FWF and in part by funds provided by the U.S. Department of Energy (D.O.E.) under cooperative research agreement #DF-FC02-94ER40818.

Contents

I	Introduction	1
II	The θ vacuum	5
III	Instanton vacuum and zero modes	8
IV	Solution of the massless model	11
V	Vacuum functional and vacuum energy density	13
VI	Condensates, susceptibilities and confinement	19
VII	Feynman rules for mass perturbation theory	21
VIII	The Schwinger mass	23
IX	Dyson-Schwinger equations and exact n-point functions	27
	A Two-point function	28
	B Higher n -point functions	30
X	Bound-state masses and decay widths	34
	A General bound-state structure	34
	B n -boson bound-state masses	37
	C A mixed bound-state mass	41
	D Decay width computations	43
XI	Scattering	45
	A Two-dimensional kinematics	45
	B Scattering processes	46
XII	Summary	52

I. INTRODUCTION

The massless and massive Schwinger models are two-dimensional QED with one massless or massive fermion. Both models have been subject to intensive study in the last decades. First of all, the exact solubility of the massless Schwinger model was discovered by J. Schwinger more than 30 years ago [1]. Later on, Lowenstein and Swieca [2] constructed a complete operator solution of the massless model. By carefully investigating the role of large gauge transformations they found that these large gauge transformations have the effect of changing the vacuum ("instanton vacuum"), and therefore a superposition of all these vacua (" θ vacuum") has to be introduced as a new, physical vacuum in order to render the theory sensible (requirement of vacuum clustering). In the usual terminology of gauge theories, the occurrence of instanton-like gauge-field configurations can be traced back to the fact that

the boundary of Euclidean space-time is a S^1 , and, further, that the first homotopy group of the gauge group is nontrivial, $\Pi_1(U(1)) = \mathbf{Z}$.

In addition, the chiral anomaly and Schwinger terms are present in these models, and all these nontrivial field-theoretical features were one reason for the rising interest in the Schwinger model [7,8], [11] – [14], [17,41].

However, there is another reason for the study of the Schwinger model, namely its similarity to some aspects of QCD. All the above-mentioned features are present in QCD, too. In addition, a fermion condensate is formed both in QCD and in the massless and massive Schwinger models [3,4,18,21], and confinement is realized in the latter models in a quite understandable way. In both models there are no fermions in the physical particle spectrum. The lowest physical state is a massive mesonic fermion-antifermion bound state, the Schwinger boson. In the massless model this boson is free, and higher states are trivial free n -particle states. In the massive model these states turn into n -boson bound states, because the Schwinger boson is an interacting particle there [25,28,34,35].

When confinement properties are tested with external charges, the two models behave differently, too. In the massless model widely separated probe charges are completely screened via vacuum polarization, and the potential between the external charges approaches a constant.

For the massive model this screening takes place as long as the probe charges g are integer multiples of the fundamental fermion charge e . When $g \neq ne$, the potential between the probe charges rises linearly for large distances. So "screening" is realized in the massless model, whereas true confinement takes place in the massive model (this feature was first discovered in [24] within a bosonization approach, and is further discussed e.g. in [44,11,39]; see also Section 6). Therefore, the Schwinger model was studied in order to get more insight into the phenomena of quark trapping and confinement [11,15,16].

Instanton physics was studied, too, in the Schwinger model [22,23].

In addition, because of its simplicity, the Schwinger model is often used for testing some new methods of QFT, like light-cone quantization [46] – [51], semi-classical methods [11,33,44] or lattice calculations [52] – [57].

As mentioned, the massless Schwinger model was first completely solved within the operator formalism [2], and the operator approach and the specific two-dimensional method of bosonization were mainly used in the subsequent years [15,16,24,25,9]. It took some time until a path integral approach to the Schwinger model arose (mainly because of the problems with the nontrivial vacuum structure) [10], [36] – [38], [3] – [6], [18] – [20].

In this article all computations are based on the path integral formalism in flat Euclidean space-time.

This article is organized as follows:

After fixing our conventions we discuss some general features and the physical meaning of the vacuum angle θ . Then we turn to the massless model, because it will be the starting point for a mass perturbation theory. We discuss the relevance of the instanton vacuum and briefly review the exact path integral solution of the massless model to the accuracy we need in the sequel.

In a next step we compute the vacuum functional and vacuum energy density of the massive model in mass perturbation theory by a method that is analogous to the cluster

expansion of statistical physics. Further we prove the IR finiteness of the mass perturbation theory and comment on the UV regularization.

With the help of the vacuum energy density we compute the fermion and photon condensates and the scalar and topological susceptibilities and generalize (to arbitrary order mass perturbation theory) some recent path integral computations [44] on screening and confinement in the massive Schwinger model.

Then we develop the Feynman rules for the mass perturbation theory, which we need in the sequel. Actually, because of the chiral properties of the model these Feynman rules acquire a matrix structure.

Further we compute the mass of the Schwinger boson by a direct application of this mass perturbation theory.

From the equations of motion we derive, in Section 9, the Dyson-Schwinger equations of the model and use them to re-express the exact n -point functions in a way that is more suitable for the subsequent discussion of bound states, decays and scattering. From the exact two-point function we will be able to infer the complete bound-state spectrum of the model and find that it contains, in addition to the n -boson bound states, some further bound states (Section 10).

Further, this exact two-point function provides information on the decay widths of all the unstable bound states. As an illustration, we will compute the masses and decay widths of the lowest bound states.

At last, we discuss the scattering processes of the model, where we take properly into account all the resonances and higher production thresholds. All this may be derived from a resummed mass perturbation theory, without further approximations.

We will use the following conventions,

$$g_{\mu\nu} = \delta_{\mu\nu} \quad , \quad \epsilon_{01} = -i \quad , \quad \epsilon_{\mu\nu}\epsilon^{\nu\lambda} = g_{\mu}^{\lambda} \quad (1)$$

$$\gamma_{\mu}\gamma_5 = \epsilon_{\mu\nu}\gamma^{\nu} \quad , \quad \text{tr}\gamma_5\gamma_{\mu}\gamma_{\nu} = -2\epsilon_{\mu\nu} \quad , \quad \gamma_5 = -i\gamma^0\gamma^1 \quad (2)$$

$$\gamma^0 = \begin{pmatrix} 0 & i \\ -i & 0 \end{pmatrix} \quad , \quad \gamma^1 = \begin{pmatrix} 0 & 1 \\ 1 & 0 \end{pmatrix} \quad , \quad \gamma_5 = \begin{pmatrix} 1 & 0 \\ 0 & -1 \end{pmatrix} \quad (3)$$

and we find it convenient to keep the notation (x_0, x_1) in Euclidean space-time. As a consequence, the dual field strength pseudoscalar

$$F = \frac{1}{2}\epsilon_{\mu\nu}F^{\mu\nu} = \frac{1}{e}\square\beta \quad (4)$$

is imaginary (β is defined in (6)). The Lagrangian of Euclidean QED₂ is

$$L = \bar{\Psi}(i\rlap{\not{D}} - e\rlap{\not{A}} + m)\Psi - \frac{1}{4}F_{\mu\nu}F^{\mu\nu} \quad (5)$$

and we use the following representation for the gauge field

$$A_{\mu}(x) = \frac{1}{e}(\partial_{\mu}\alpha(x) + \epsilon_{\mu\nu}\partial^{\nu}\beta(x)). \quad (6)$$

The pure gauge part, α , is unimportant for gauge invariant VEVs (as we deal with throughout the article) and may therefore be set equal to zero, $\alpha \equiv 0$ (Lorentz condition). Using the electric charge e (which has the dimension of mass in two space-time dimensions) we define the Schwinger mass

$$\mu_0^2 = \frac{e^2}{\pi} \quad (7)$$

which is the mass of the Schwinger boson in the massless Schwinger model. Further we need the currents

$$J_\mu = \bar{\Psi}\gamma_\mu\Psi \quad , \quad J_\mu^5 = \bar{\Psi}\gamma_\mu\gamma_5\Psi = \epsilon_{\mu\nu}J^\nu$$

$$S = \bar{\Psi}\Psi \quad , \quad P = \bar{\Psi}\gamma_5\Psi$$

$$S_\pm = \bar{\Psi}P_\pm\Psi \quad , \quad P_\pm = \frac{1}{2}(1 \pm \gamma_5) \quad (8)$$

and define the Schwinger boson field, Φ , by

$$J_\mu =: \frac{1}{\sqrt{\pi}}\epsilon_{\mu\nu}\partial^\nu\Phi. \quad (9)$$

On the quantized theory the following equations of motion hold (more precisely, they hold on the physical subspace, see the remark after (103)),

$$\partial_\mu F^{\mu\nu} = eJ^\nu \quad (10)$$

$$\partial^\mu J_\mu^5 = \frac{e}{\pi}F - 2imP, \quad (11)$$

which are the Maxwell and anomaly equations. In addition, the Dirac equation holds, but we do not need it.

We use the following Feynman propagators:

massless scalar propagator

$$D_0(x) = \frac{1}{4\pi} \ln(x^2 - i\epsilon) \quad , \quad \square D_0(x) = \delta(x) \quad (12)$$

massless fermion propagator

$$G_0(x) = \frac{x^\mu \gamma_\mu}{2\pi(x^2 - i\epsilon)} = \not{x} D_0(x), \quad (13)$$

massive scalar propagator

$$D_\mu(x) = -\frac{1}{2\pi} K_0(\mu|x|) \quad , \quad \widetilde{D}_\mu(p) = \frac{-1}{p^2 + \mu^2} \quad (14)$$

and K_0 is the McDonald function with the properties

$$K_0(z) \rightarrow -\gamma - \ln \frac{z}{2} + o(z^2) \quad \text{for } z \rightarrow 0$$

$$K_0(z) \rightarrow \sqrt{\frac{\pi}{2z}} e^{-z} \quad \text{for } z \rightarrow \infty \quad (15)$$

where γ is the Euler constant.

In the sequel we will have to distinguish between two types of VEVs, namely VEVs with respect to the massless and massive Schwinger models. The former VEVs are always denoted by $\langle \rangle_0$, the latter ones sometimes by $\langle \rangle_m$ and sometimes without a subscript, $\langle \rangle$.

Here we should add a last comment on our Euclidean conventions. They are chosen in such a way that they are as similar as possible to their 1+1 Minkowski-space counterparts. However, for this advantage we have to pay the prize that in the intermediate Euclidean computations some quantities are unphysical (e.g. imaginary field strength F and vacuum angle θ).

II. THE θ VACUUM

Let us briefly recall the way the vacuum angle θ enters the theory. The key observation is the existence of large gauge transformations G_i that do not leave the vacuum invariant and therefore give rise to an infinite number of vacua,

$$G_1|0\rangle =: |1\rangle \quad , \quad G_n|0\rangle = (G_1)^n|0\rangle =: |n\rangle \quad (16)$$

and n is restricted to integer values by the requirement that gauge transformations must act uniquely on the matter fields (here the fermion). As a consequence, gauge fields may exist that tend to different pure gauges $G_{n\pm}$ for the time $t \rightarrow \pm\infty$. They have instanton number $k = n_+ - n_-$, and this instanton number may be computed from the Pontryagin index density $\nu(x)$,

$$\nu = \int dx \nu(x) = -\frac{ie}{2\pi} \int dx F(x) = k. \quad (17)$$

These instantons induce transitions between different, gauge equivalent vacua (16). Therefore, a superposition of these vacua has to be introduced as a new, physical vacuum,

$$|\theta\rangle = \sum_{n=-\infty}^{\infty} e^{in\theta} |n\rangle \quad , \quad G_n|\theta\rangle = e^{-in\theta} |\theta\rangle \quad (18)$$

$$\langle \theta' | \hat{O} | \theta \rangle = \delta(\theta - \theta') \sum_{k=-\infty}^{\infty} e^{ik\theta} \langle 0 | \hat{O} | k \rangle \quad (19)$$

and in (19) we used $\langle m | \hat{O} | n \rangle = \langle 0 | \hat{O} | n - m \rangle$, which holds for gauge invariant operators \hat{O} . Because all θ vacua are invariant with respect to large gauge transformations, up to a phase, (18), the angle θ has to be included as a new physical parameter into the theory.

From (19) we find that within the path integral approach the vacuum angle θ may be included, e.g. for the vacuum functional of the massive Schwinger model, like

$$Z(m, \theta) = \sum_{k=-\infty}^{\infty} e^{ik\theta} \int DA_k^\mu D\bar{\Psi} D\Psi e^{\int dx [\bar{\Psi}(i\partial - eA + m)\Psi - \frac{1}{4}F_{\mu\nu}F^{\mu\nu}]} \quad (20)$$

$$= \sum_{k=-\infty}^{\infty} \int DA_k^\mu D\bar{\Psi} D\Psi e^{\int dx [\bar{\Psi}(i\partial - eA + m)\Psi + \frac{1}{2}F^2 + \frac{e\theta}{2\pi}F]} \quad (21)$$

(where we used (17)) and A_k^μ has instanton number k . Due to the anomaly there is a third representation for $Z(m, \theta)$. By performing a constant chiral transformation on the fermions,

$$\Psi \rightarrow e^{i\beta\gamma_5}\Psi \quad , \quad \bar{\Psi} \rightarrow \bar{\Psi}e^{i\beta\gamma_5}, \quad (22)$$

the change of the fermionic path integral causes the anomaly,

$$\mathbf{A} = -\frac{e}{\pi}\beta \int dx F, \quad (23)$$

and in the action only the mass term is changed by this transformation. Choosing $\beta = -\frac{\theta}{2}$, the θF term is cancelled and we find

$$Z(m, \theta) = \sum_{k=-\infty}^{\infty} \int DA_k^\mu D\bar{\Psi} D\Psi e^{\int dx [\bar{\Psi}(i\partial - eA)\Psi + m \cos \theta \bar{\Psi}\Psi + im \sin \theta \bar{\Psi}\gamma_5\Psi + \frac{1}{2}F^2]} \quad (24)$$

Rewriting the θ -dependent part of (24) like

$$m(\cos \theta S + i \sin \theta P) = m(e^{i\theta} S_+ + e^{-i\theta} S_-) \quad (25)$$

we conclude that general VEVs will not be holomorphic in $me^{i\theta}$ but depend on its complex conjugate, too, $\langle \rangle_m(me^{i\theta}, me^{-i\theta})$.

There is a nice physical interpretation of θ that was extensively discussed in [25], which we want to present now. Ignoring the fermions at the moment and treating F as the fundamental field in (21), we find the equation of motion

$$F = -\frac{e\theta}{2\pi}. \quad (26)$$

So θ may be interpreted as a constant background electric field.

[*Remark:* There is a simple and very instructive way of discussing this feature in the Schrödinger picture, which we want to describe briefly (this was shown to us by R. Jackiw). The Hamiltonian of the theory without fermion reads, in the gauge $A_0 = 0$ (remember that A_0 has no conjugate momentum; $F = \partial_0 A_1$; we temporarily introduce a finite length L for the space direction x_1)

$$H = \frac{1}{2} \int_0^L dx_1 F^2$$

The quantum theory is described in the Schrödinger picture by operators $A_1(x)$ and $\hat{F}(x) \equiv i\frac{\delta}{\delta A_1(x)}$ acting on wave functionals $\Psi[A_1]$. The Gauss law for physical states simply reads

$$\partial_1 \hat{F}(x) \Psi[A_1] \equiv \partial_1 i \frac{\delta}{\delta A_1(x)} \Psi[A_1] = 0$$

with the general solution

$$\Psi[A_1] = f(a) \quad , \quad a := \int_0^L dx_1 A_1(x)$$

where f is an arbitrary function. So there remains only one degree of freedom (the zero Fourier component of A_1). The Schrödinger equation reads ($E \dots$ energy)

$$\frac{1}{2} \int_0^L dx_1 \hat{F}^2(x) f(a) \equiv -\frac{1}{2} \int_0^L dx_1 \frac{\delta^2}{\delta A_1^2(x)} f(a) = E f(a)$$

with the solution

$$f(a) = e^{-iFa} \quad , \quad E = \int_0^L dx_1 \frac{F^2}{2} = L \frac{F^2}{2},$$

where F is the eigenvalue of \hat{F} ,

$$\hat{F} f(a) = \langle \hat{F} \rangle f(a) =: F f(a)$$

So F is just a constant field with energy density $\frac{F^2}{2}$. Finally, when we perform a large gauge transformation $eA_1 \rightarrow eA_1 - \partial_1 \lambda$, $\lambda(L) = \lambda(0) + 2\pi n$, $\Psi[A_1]$ changes according to

$$\Psi[A_1 - \frac{1}{e} \partial_1 \lambda] = \Psi[A_1] e^{\frac{2\pi i n}{e} F}$$

Therefore, the state vector $\Psi[A_1]$ changes under large gauge transformations precisely like the θ vacuum (18), provided we make the identification $F = -\frac{e\theta}{2\pi}$, equ. (26), which again shows that θ is a constant background field.]

When matter is included, it was shown in [25] that whenever $\theta > \pi$ ($\theta < -\pi$), it is energetically favourable to create a real particle-antiparticle pair (with fundamental charge $\pm e$) that partially screens the background field (26). This explains the angular character of θ .

Quantum effects further change the picture. For the massless Schwinger model ($m = 0$) it is obvious from (24) that the background field is completely screened. The anomaly (23) stems from the vacuum polarization graph in QED₂ (for a lengthy discussion and explicit computation of the QED₂-anomaly see e.g. [17,19]), therefore the screening is due to vacuum polarization. In the massive case this screening is not complete and we will find (see Section 6)

$$\langle F \rangle_m \sim -m \sin \theta + o(m^2). \quad (27)$$

III. INSTANTON VACUUM AND ZERO MODES

The following two sections are devoted to a short review of some properties of the massless Schwinger model which we need in the sequel. First we remember that the exact fermion propagator in an external gauge field may be given explicitly,

$$G^\beta(x, y) = e^{i\gamma_5(\beta(x) - \beta(y))} G_0(x - y) \quad (28)$$

(more precisely, (28) is correct for gauge fields with vanishing instanton number, $k = 0$. For $k \neq 0$ G^β acquires an additional term. This term, however, does not contribute to the path integral computations which we want to perform and may therefore be omitted, see the remark after (32)).

Further we should recapitulate some wellknown properties of the Dirac operator in an instanton field. For sufficiently simple space-time manifolds the Dirac operator

$$\mathcal{D} = \not{\partial} + ie\not{A} \quad (29)$$

in a gauge field with instanton number k has precisely $|k|$ zero modes, which have positive chirality for $k > 0$ and negative chirality otherwise. For the Schwinger model these zero modes may be computed explicitly (see [18,19]),

$$\begin{aligned} \Psi_{i_0}^{\beta_k} &= \frac{1}{\sqrt{2\pi}} (x^-)^{i_0} e^{i\beta_k} \begin{pmatrix} 1 \\ 0 \end{pmatrix} \quad , \quad k > 0 \quad , \quad i_0 = 0 \dots k-1, \\ \Psi_{i_0}^{\beta_k} &= \frac{1}{\sqrt{2\pi}} (x^+)^{i_0} e^{-i\beta_k} \begin{pmatrix} 0 \\ 1 \end{pmatrix} \quad , \quad k < 0 \quad , \quad i_0 = 0 \dots |k|-1, \end{aligned} \quad (30)$$

$$x^+ = x_1 + ix_0 \quad , \quad x^- = x_1 - ix_0.$$

Next let us investigate the pure fermionic part of the path integral in an external gauge field (for a proper treatment of the zero modes we keep a small fermion mass m that we set equal to zero at the end of the computation).

Because of the identity

$$\begin{aligned} Z[A_\mu^k] &= \lim_{m \rightarrow 0} \int D\bar{\Psi} D\Psi e^{\int dx \bar{\Psi}(i\mathcal{D}+m)\Psi} \\ &= \lim_{m \rightarrow 0} \det(i\mathcal{D}+m) = \lim_{m \rightarrow 0} m^{|k|} \det'(i\mathcal{D}+m) \end{aligned} \quad (31)$$

the vacuum functional obviously vanishes for $k \neq 0$ (the prime indicates omission of the zero eigenvalues).

This remains true for VEVs of operators containing only gauge fields, because they do not influence the fermionic integration. On the other hand, fermionic VEVs may get contributions from nontrivial instanton sectors.

By the use of Grassmann integration rules a general fermionic VEV may be written like

$$\langle \Psi^{\alpha_1}(x_1) \bar{\Psi}^{\beta_1}(y_1) \dots \Psi^{\alpha_n}(x_n) \bar{\Psi}^{\beta_n}(y_n) \rangle_0 [A_\mu^k] =$$

$$\lim_{m \rightarrow 0} \sum_{\pi(1 \dots n)} (-)^{\sigma(\pi)} \prod_{i=1}^n \sum_{l_i} \frac{\psi_{l_i}^{\alpha_i}(x_i) \bar{\psi}_{l_i}^{\beta_{\pi(i)}}(y_{\pi(i)})}{i\lambda_{l_i} + m} m^{|k|} \prod_l' (i\lambda_l + m). \quad (32)$$

Here $\psi_l(x)$ and λ_l denote eigenfunctions and eigenvalues of the Dirac operator, and the sum just means summation of all possible Wick contractions (for a more detailed discussion see e.g. [3,18,19]).

This expression may give a nonvanishing result when in precisely $|k|$ Green functions only zero modes contribute, because then the $m^{|k|}$ factor is cancelled by a factor $m^{-|k|}$. Of course, every zero mode has to occur exactly once because of the Pauli principle (the Pauli principle is not explicitly written down in (32); however, because of the permutation sign factor $(-)^{\sigma(\pi)}$ there is a pair-wise cancellation of all terms with identical eigenfunctions). Therefore, a VEV of n fermion bilinears, like (32), may get contributions from instanton sectors $k = -n, \dots, n$.

[*Remark:* for a nontrivial instanton sector $k \neq 0$, the remaining Green functions in (32) (the exact fermion propagators (28)) in principle should be constructed on the subspace that is orthogonal to the zero modes, i.e. they should satisfy

$$\not{D}_x^{\beta_k} G^{\beta_k}(x, y) = \mathbf{1} \delta(x - y) - \sum_{i_0=0}^{|k|-1} c_{i_0} \Psi_{i_0}^{\beta_k}(x) \bar{\Psi}_{i_0}^{\beta_k}(y)$$

and, consequently, read

$$\begin{aligned} G^{\beta_k}(x, y) &= e^{i\gamma_5 \beta_k(x)} G_0(x - y) e^{i\gamma_5 \beta_k(y)} - e^{i\gamma_5 \beta_k(x)} \sum_{i_0=0}^{|k|-1} c_{i_0} \chi_{i_0}^{\beta_k}(x) \bar{\Psi}_{i_0}^{\beta_k}(y) \\ &= e^{i\gamma_5 \beta_k(x)} G_0(x - y) e^{i\gamma_5 \beta_k(y)} - \sum_{i_0=0}^{|k|-1} c_{i_0} \Psi_{i_0}^{\beta_k} \bar{\chi}_{i_0}^{\beta_k}(y) e^{i\gamma_5 \beta_k(y)} \end{aligned}$$

where

$$\not{\partial}_x \chi_{i_0}^{\beta_k}(x) = e^{i\gamma_5 \beta_k(x)} \Psi_{i_0}^{\beta_k}(x) \quad , \quad \partial^\mu \bar{\chi}_{i_0}^{\beta_k}(y) \gamma_\mu = \bar{\Psi}_{i_0}^{\beta_k}(y) e^{i\gamma_5 \beta_k(y)}$$

(the c_{i_0} are related to the zero mode normalizations and are unimportant for our argument). The important point is, of course, that the additional term for G^{β_k} contains the zero modes and, therefore, does not contribute to the fermionic path integral (32) due to the Pauli principle. As a consequence, in our computations we may use the simple form (28) of the exact fermion propagator for all instanton sectors (this argument can be found e.g. in [31]).

For further conclusions we have to specify the types of fermionic bilinears. E.g. pure vector-like VEVs get contributions only from the trivial sector $k = 0$ for the following reason: the zero modes contribute like $\Psi_{i_0} \bar{\Psi}_{i_0} \sim P_+$ (for $k > 0$), the exact propagators are given in (28), and therefore all vector-like VEVs look like (for $k > 0$)

$$\text{tr} P_+ \gamma_{\mu_1} G_2^\beta \gamma_{\mu_2} G_3^\beta \gamma_{\mu_3} \dots = 0$$

$$\text{tr} P_+ \gamma_{\mu_1} P_+ \gamma_{\mu_2} G_3^\beta \gamma_{\mu_3} \dots = \text{tr} P_+ P_- \gamma_{\mu_1} \gamma_{\mu_2} \dots = 0 \quad , \quad \text{etc.}$$

and therefore vanish.

On the other hand, VEVs of scalar or chiral bilinears do get contributions from the $k \neq 0$ sectors.

For densities, like $S(x) = \bar{\Psi}(x)\Psi(x)$ (which are the only objects we need in the sequel), this may be inferred in a very easy fashion from the various representations of the vacuum functional, (20) - (24). Suppose for the moment that the fermion mass is space-time dependent. Then the scalar VEVs of the massless model are given by (see (20))

$$\begin{aligned} \langle \prod_{i=1}^n \bar{\Psi}(x_i)\Psi(x_i) \rangle_0 &= \frac{1}{Z(0, \theta)} \prod_{i=1}^n \frac{\delta}{\delta m(x_i)} Z[m(x), \theta]|_{m=0} = \langle \prod_{i=1}^n (e^{i\theta} S_+(x_i) + e^{-i\theta} S_-(x_i)) \rangle_0^{\theta=0} \\ &= e^{in\theta} \langle \prod_{i=1}^n S_+(x_i) \rangle_0^{\theta=0} + e^{i(n-2)\theta} \sum_{j=1}^n \langle S_-(x_j) \prod_{\substack{i=1 \\ i \neq j}}^n S_+(x_i) \rangle_0^{\theta=0} + \dots + e^{-in\theta} \langle \prod_{i=1}^n S_-(x_i) \rangle_0^{\theta=0} \end{aligned} \quad (33)$$

where we used (24), (25) in the first line.

Further we know from (20) that a factor $e^{ik\theta}$ indicates that the term stems from the instanton sector k . Therefore, we may draw the conclusion that for a n -scalar VEV the sectors $k = n, n-2, \dots, -n$ contribute. In addition, we find that for a VEV of n_+ positive chirality densities S_+ and n_- negative chirality densities S_- only the sector $k = n_+ - n_-$ contributes and that “instanton number equals chirality”.

[*Remark:* we gave a quite explicit construction of the vacuum structure of the massless Schwinger model, because we need it for our further calculations. However, if one is only interested in the vacuum structure itself, it may be shown to be an almost trivial consequence of gauge invariance. First, imposing the Lorentz gauge condition $\alpha = 0$ in the representation (6) of the gauge field does not uniquely fix the gauge. There remains a residual gauge freedom to introduce functions β that fulfill the condition $\square\beta = 0$. Of course, a constant $\beta = c$ is a possible choice. Requiring gauge invariance and using the anomaly result (23) (for a constant chiral rotation c) we find for the vacuum functional

$$\int D\bar{\Psi}D\Psi D\beta e^{S[\bar{\Psi}, \Psi, \beta]} \equiv \int D\bar{\Psi}D\Psi D\beta e^{S[\bar{\Psi}e^{ic\gamma_5}, e^{ic\gamma_5}\Psi, \beta]} = \int D\bar{\Psi}D\Psi D\beta e^{S[\bar{\Psi}, \Psi, \beta] - 2ic\frac{ie}{2\pi} \int dx F}$$

and conclude $\nu = \frac{-ie}{2\pi} \int dx F = 0$. Therefore, for the vacuum functional only the sector $k = 0$ may contribute. The conclusion remains the same for gauge field VEVs and for vector current VEVs. For scalar and chiral VEVs, however, things change. E.g. for the positive chiral VEV $\langle S_+(x) \rangle_0$ we find

$$\int D\bar{\Psi}D\Psi D\beta \bar{\Psi}(x)P_+\Psi(x)e^{S[\bar{\Psi}, \Psi, \beta]} \equiv \int D\bar{\Psi}D\Psi D\beta \bar{\Psi}(x)e^{ic\gamma_5}P_+e^{ic\gamma_5}\Psi(x)e^{S[\bar{\Psi}, \Psi, \beta] - 2ic\nu}$$

and conclude $(\gamma_5 P_+ = P_+ \gamma_5 = P_+)$ that $\nu = 1$. Therefore, here only the sector $k = 1$ may contribute. The generalization to higher VEVs is straight forward, and we may indeed conclude that the vacuum structure of the Schwinger model is a consequence of gauge invariance. (For the massive model the same gauge invariance requirement leads to the equivalence of the different representations (21), (24) for the vacuum functional $Z(m, \theta)$. A similar discussion can be found in [26], and more about instantons and θ vacua e.g. in [58].)

IV. SOLUTION OF THE MASSLESS MODEL

The key observation for the exact solution of the massless model is the fact that the interaction term in the fermionic Lagrangian may be transformed away by a chiral rotation ($A_\mu = \epsilon_{\mu\nu} \partial^\nu \beta$),

$$L_\Psi = \bar{\Psi}(i\partial - eA)\Psi = \bar{\Psi}e^{-i\beta\gamma_5}i\partial e^{-i\beta\gamma_5}\Psi. \quad (34)$$

In the fermionic path integral such a chiral rotation causes the chiral anomaly. In the model at hand this anomaly may be computed for finite chiral rotations, too, leading to the result for general VEVs (for $\theta = 0$; N is the path integral normalization)

$$N \int D\bar{\Psi}D\Psi D\beta \hat{O}(\Psi, \bar{\Psi}, \beta) e^S =$$

$$N \int D\bar{\Psi}_f D\Psi_f D\beta e^{\int dx \bar{\Psi}_f i\partial \Psi_f} \hat{O}(e^{i\beta\gamma_5} \Psi_f, \bar{\Psi}_f e^{i\beta\gamma_5}, \beta) e^{S_{\text{eff}}} \quad (35)$$

where

$$S_{\text{eff}} = \frac{1}{2e^2} \int dx [(\square\beta)^2 - \frac{e^2}{\pi} \beta \square\beta] =: \int dx \beta \mathbf{D}\beta \quad (36)$$

$$\mathbf{D} = \frac{\square}{e^2} (\square - \mu_0^2) \quad , \quad \mathbf{G}(x) = \pi(D_{\mu_0}(x) - D_0(x)) \quad , \quad \mathbf{D}_x \mathbf{G}(x - y) = \delta(x - y). \quad (37)$$

The first term in S_{eff} is the "photon" kinetic energy, the second one stems from the anomaly; Ψ_f is the free fermion spinor.

For a further evaluation the presence of zero modes for $k \neq 0$ has to be taken into account. In $\hat{O}(\Psi, \bar{\Psi}, \beta)$ all Wick contractions among the fermions $\Psi = e^{i\beta\gamma_5} \Psi_f$ have to be done and the corresponding number of k zero modes and remaining $n - k$ exact propagators have to be inserted, according to our discussion in the last section. All this may be written down in a compact way by introducing the generating functional for fermions in the instanton sector k ,

$$Z_k[\bar{\eta}, \eta] = e^{ik\theta} N \int D\beta_k \prod_{i_0=0}^{k-1} (\bar{\eta} | \Psi_{i_0}^{\beta_k}) (\bar{\Psi}_{i_0}^{\beta_k} | \eta) e^{-i \int dx dy \bar{\eta}(x) G^{\beta_k}(x, y) \eta(y)} e^{S_{\text{eff}}}, \quad (38)$$

where $\eta, \bar{\eta}$ are Grassmann-valued external spinor sources.

Both exact propagator (28) and zero modes (30) depend exponentially on β , therefore they add linear β terms to S_{eff} , rendering thereby the β path integral Gaussian. As a consequence, all VEVs may be computed explicitly, as we now demonstrate briefly.

E.g. for the chiral density $\langle S_+(x) \rangle_0$ only the $k = 1$ sector contributes; we have to insert one zero mode (30) and find

$$\langle S_+(x) \rangle_0 = e^{i\theta} N \int D\beta \text{tr} P_+ \frac{1}{2\pi} e^{i(\beta(x) + \beta(x))} P_+ e^{\int dz \beta \mathbf{D}\beta} =$$

$$\frac{e^{i\theta}}{2\pi} e^{2\mathbf{G}(0)} = e^{i\theta} \frac{e^\gamma \mu_0}{4\pi} =: e^{i\theta} \frac{\Sigma}{2} \quad (39)$$

where we completed the square and performed the β integration in the first step; further we introduced the fermion condensate

$$\Sigma \equiv \langle \bar{\Psi}(x) \Psi(x) \rangle_0^{\theta=0} = \frac{e^\gamma \mu_0}{2\pi}. \quad (40)$$

Analogously we find for the two-point functions

$$\langle S_+(x) S_-(y) \rangle_0 = -N \int D\beta e^{\int dz \beta \mathbf{D}\beta}.$$

$$\cdot \text{tr} e^{2i\gamma_5(\beta(x)-\beta(y))} P_+ G_0(x-y) P_- G_0(y-x) =$$

$$\frac{e^{4(\mathbf{G}(0)-\mathbf{G}(x-y))}}{4\pi^2(x-y)^2} = \left(\frac{e^\gamma \mu_0}{4\pi}\right)^2 e^{-4\pi D_{\mu_0}(x-y)} \quad (41)$$

(here only one of the two possible Wick contractions contributed due to $\text{tr} P_+ G = 0$) and

$$\langle S_+(x) S_+(y) \rangle_0 = \dots = e^{2i\theta} \frac{(x-y)^2}{4\pi^2} e^{4(\mathbf{G}(0)+\mathbf{G}(x-y))} = e^{2i\theta} \left(\frac{e^\gamma \mu_0}{4\pi}\right)^2 e^{4\pi D_{\mu_0}(x-y)}. \quad (42)$$

(the details of all these computations can be found e.g. in [18,19]).

Observe that in both cases the massless propagator part of $\mathbf{G}(x-y)$ is cancelled by a contribution stemming from the free fermion propagator or from the zero modes, respectively. This feature remains true for all physical VEVs and shows that the only physical particle in the Schwinger model is the massive Schwinger boson.

Further it may be seen easily that all VEVs fulfill the vacuum clustering property, e.g.

$$\lim_{x-y \rightarrow \infty} \langle S_\pm(x) S_\pm(y) \rangle_0 = \langle S_\pm(x) \rangle_0 \langle S_\pm(y) \rangle_0. \quad (43)$$

In fact, vacuum clustering is another reason that makes it necessary to introduce an instanton vacuum.

The above calculations may be easily generalized to higher VEVs of chiral densities. The general formula reads (see e.g. [31])

$$\langle S_{H_1}(x_1) \cdots S_{H_n}(x_n) \rangle_0 = e^{ik\theta} \left(\frac{\Sigma}{2}\right)^n \exp \left[\sum_{i < j} \sigma_i \sigma_j 4\pi D_{\mu_0}(x_i - x_j) \right] \quad (44)$$

$$k = \sum_{i=1}^n \sigma_i = n_+ - n_-$$

where $\sigma_i = \pm 1$ for $H_i = \pm$. This result we need for the mass perturbation theory.

Further VEVs that may be easily found are the field strength VEV

$$\langle F(x)F(y) \rangle_0 = \frac{1}{e^2} \square_x \square_y \langle \beta(x)\beta(y) \rangle_0 = -\mu_0^2 D_{\mu_0}(x-y) - \delta(x-y) \quad (45)$$

and the vector current correlator. For the latter it is most efficient to introduce a vector current source into the path integral,

$$eB_\mu = \epsilon_{\mu\nu} \partial^\nu b \quad (46)$$

$$eB_\mu J^\mu = \frac{1}{\sqrt{\pi}} \epsilon_{\mu\nu} \partial^\nu b \epsilon^{\mu\lambda} \partial_\lambda \Phi = \frac{1}{\sqrt{\pi}} \Phi \square b =: \Phi \lambda \quad (47)$$

where $\lambda = \frac{1}{\sqrt{\pi}} \square b$ is the source for the Schwinger boson Φ . Now the inclusion of the source consists in the substitution $\beta \rightarrow \beta + b$ in the second (anomaly) term of the effective action (36) and in the exact fermion propagators (28) and zero modes (30). The remaining path integral computation is similar to the one which we discussed previously and leads to the following VEVs (for n chiral densities, which are at the same time generating functionals for the Schwinger boson)

$$\begin{aligned} \langle S_{H_1}(x_1) \cdots S_{H_n}(x_n) \rangle_0[\lambda] &= e^{ik\theta} \left(\frac{\Sigma}{2} \right)^n \exp \left[\sum_{i < j} \sigma_i \sigma_j 4\pi D_{\mu_0}(x_i - x_j) \right] \\ &\cdot \exp \left[- \int dy_1 dy_2 \lambda(y_1) D_{\mu_0}(y_1 - y_2) \lambda(y_2) + 2i\sqrt{\pi} \sum_{l=1}^n \sigma_l \int dy \lambda(y) D_{\mu_0}(y - x_l) \right] \end{aligned} \quad (48)$$

(for an explicit computation see [33]).

Observe that, although b was needed in the intermediate computations, the final result can be expressed entirely in terms of λ , and only massive propagators occur. This again shows that the massive Schwinger boson is the only physical particle of the theory.

After this short discussion and formulae collection of the massless Schwinger model we are prepared for the mass perturbation expansion of the massive model. This will be done in the forthcoming sections.

V. VACUUM FUNCTIONAL AND VACUUM ENERGY DENSITY

By simply expanding the mass term in (20), $e^m \int dx \bar{\Psi} \Psi$, the Euclidean vacuum functional for the massive Schwinger model may be traced back to VEVs of the massless model and some space-time integrations ([27]),

$$Z(m, \theta) = \sum_{n=0}^{\infty} \frac{m^n}{n!} \int dx_1 \cdots dx_n \langle \prod_{i=1}^n \bar{\Psi}(x_i) \Psi(x_i) \rangle_0 \quad (49)$$

where $\langle \prod_{i=1}^n S(x_i) \rangle_0 = \langle \prod_{i=1}^n (S_+(x_i) + S_-(x_i)) \rangle_0$ may be inferred from (44). There, all contractions among $S_{H_i}(x_i) S_{H_j}(x_j)$ produce exponentials of the massive propagator $D_{\mu_0}(x_i - x_j)$. For a first, rough approximation we may use the fact that the massive scalar propagator $D_{\mu_0}(x)$ vanishes exponentially for large argument. Therefore, when integrating over space

time and expanding the exponential, all contributions from $D_{\mu_0}^l$ will be ignored for the moment, supposing that the space time volume V is sufficiently large. In this case the integrations in (49) just produce factors of V . Further, when inserting (44) into (49) we have to sum over all possible distributions of $n_+ = n - n_-$ pluses and n_- minuses on n scalar densities S . This results in a factor $\binom{n}{n_-}$. Therefore we find for the n -th order term

$$\langle \prod_{i=1}^n \int dx_i S(x_i) \rangle \sim \left(\frac{\Sigma}{2}\right)^n V^n \sum_{n_-=0}^n \binom{n}{n_-} e^{i(n-2n_-)\theta} = (\Sigma V \cos \theta)^n \quad (50)$$

and for the normalized vacuum functional

$$\frac{Z(m, \theta)}{Z(0, 0)} \sim \exp(m \Sigma V \cos \theta) \quad (51)$$

(we ignored terms like $m^n V^{n-1}$ in this approximation compared to $m^{n-1} V^{n-1}$, therefore (51) is the first order result in m). This result is wellknown, and its consequences for the vacuum structure and spectrum of the Dirac operator are discussed in great detail in [42].

As we have seen, the exponentials $e^{\pm 4\pi D_{\mu_0}(x)}$ produce volume factors V upon integration, and, consequently, they will not lead to an IR-finite perturbation expansion for $V \rightarrow \infty$. Therefore, we have to expand the (products of) exponentials in (49) into the functions $E_{\pm}(x)$

$$E_{\pm}(x) := e^{\pm 4\pi D_{\mu_0}(x)} - 1$$

$$E_{\pm}^{(n)}(x) := e^{\pm 4\pi D_{\mu_0}(x)} - \sum_{l=0}^n \frac{1}{l!} (\pm 4\pi D_{\mu_0}(x))^l$$

$$\tilde{E}_{\pm}^{(n)}(p) = \int d^2x e^{ipx} E_{\pm}^{(n)}(x) \quad , \quad E_{\pm} := \int dx E_{\pm}(x) \quad (52)$$

(where we defined some related functions for later convenience). The $E_{\pm}(x)$ decay exponentially for large $|x|$.

Inserting the exact VEVs (44) into (49) and using the notation (52), we obtain for the vacuum functional $Z(m, \theta)$, order by order

n=1:

$$\frac{m}{1!} \frac{\Sigma}{2} \int dx (e^{i\theta} + e^{-i\theta}) = \frac{m}{1!} \frac{\Sigma}{2} V (e^{i\theta} + e^{-i\theta}) \quad (53)$$

n=2:

$$\begin{aligned} & \frac{m^2}{2!} \left(\frac{\Sigma}{2}\right)^2 \int dx_1 dx_2 \left[e^{2i\theta} e^{4\pi D_{\mu}(x_1-x_2)} + 2e^{-4\pi D_{\mu}(x_1-x_2)} + e^{-2i\theta} e^{4\pi D_{\mu}(x_1-x_2)} \right] \\ &= \frac{m^2}{2!} \left(\frac{\Sigma}{2}\right)^2 \left[V^2 (e^{2i\theta} + 2 + e^{-2i\theta}) + V (E_+ e^{2i\theta} + 2E_- + E_+ e^{-2i\theta}) \right] \end{aligned} \quad (54)$$

n=3:

$$\begin{aligned}
\ldots &= \frac{m^3}{3!} \left(\frac{\Sigma}{2} \right)^3 \left[V^3 (e^{3i\theta} + 3e^{i\theta} + 3e^{-i\theta} + e^{-3i\theta}) + \right. \\
&V^2 (3E_+ e^{3i\theta} + 3(E_+ + 2E_-) e^{i\theta} + 3(E_+ + 2E_-) e^{-i\theta} + 3E_+ e^{-3i\theta}) + \\
&V \left((3E_+^2 + E_+ \times E_+ \times E_+) (e^{3i\theta} + e^{-3i\theta}) + 3(2E_+ E_- + E_-^2 + E_+ \times E_- \times E_-) (e^{i\theta} + e^{-i\theta}) \right) \left. \right] \\
&\quad (55)
\end{aligned}$$

n=4:

$$\begin{aligned}
\ldots &= \frac{m^4}{4!} \left(\frac{\Sigma}{2} \right)^4 \left[V^4 (e^{4i\theta} + 4e^{2i\theta} + 6 + 4e^{-2i\theta} + e^{-4i\theta}) + \right. \\
&V^3 (6E_+ e^{4i\theta} + 12(E_+ + E_-) e^{2i\theta} + 12(E_+ + 2E_-) + 12(E_+ + E_-) e^{-2i\theta} + 6E_+ e^{-4i\theta}) + \\
&V^2 ((15E_+^2 + 4E_+ \times E_+ \times E_+) (e^{4i\theta} + e^{-4i\theta}) + \\
&4(3E_+^2 + 9E_+ E_- + 3E_-^2 + E_+ \times E_+ \times E_+ + 3E_+ \times E_- \times E_-) (e^{2i\theta} + e^{-2i\theta}) + \\
&+ 6(E_+^2 + 8E_+ E_- + E_-^2 + 4E_+ \times E_- \times E_-)) + \ldots \left. \right] \\
&\quad (56) \\
&\quad \ldots
\end{aligned}$$

where the cross indicates convolutions, e.g.

$$E_+ \times E_+ \times E_+ \equiv \int dy_1 dy_2 E_+(y_1) E_+(y_1 + y_2) E_+(y_2) \quad (57)$$

and we displayed the result up to the accuracy we need. Observe that the result is not obtained by just expanding polynomials like $(1 + E_+(x_i))^l$, because e.g. a third power in $E_+(x_i)$ may contribute to $V^{n-3}E_+^3$ or to $V^{n-2}E_+ \times E_+ \times E_+$. Concerning the dimensions, observe that $E_{\pm}(x)$ is dimensionless and, therefore, e.g. $[E_{\pm}] \sim [V]$, $[E_{\pm} \times E_{\pm} \times E_{\pm}] \sim [V^2]$, etc.

In a next step we rearrange the terms (53) – (56) in rising powers of V :

$$\begin{aligned}
&\frac{V}{1!} \left[m \frac{\Sigma}{2} (e^{i\theta} + e^{-i\theta}) + \frac{m^2}{2} \left(\frac{\Sigma}{2} \right)^2 (E_+ e^{2i\theta} + 2E_- + E_+ e^{-2i\theta}) + \right. \\
&\frac{m^3}{6} \left(\frac{\Sigma}{2} \right)^3 ((3E_+^2 + E_+ \times E_+ \times E_+) (e^{3i\theta} + e^{-3i\theta}) + 3(2E_+ E_- + E_-^2 + E_+ \times E_- \times E_-) (e^{i\theta} + e^{-i\theta})) + \ldots \left. \right] + \\
&\frac{V^2}{2!} \left[m^2 \left(\frac{\Sigma}{2} \right)^2 (e^{2i\theta} + 2 + e^{-2i\theta}) + m^3 \left(\frac{\Sigma}{2} \right)^3 (E_+ (e^{3i\theta} + e^{-3i\theta}) + (E_+ + 2E_-) (e^{i\theta} + e^{-i\theta})) + \right.
\end{aligned}$$

$$\begin{aligned}
& \frac{m^4}{12} \left(\frac{\Sigma}{2} \right)^4 \left((15E_+^2 + 4E_+ \times E_+ \times E_+) (e^{4i\theta} + e^{-4i\theta}) + \right. \\
& 4(3E_+^2 + 9E_+E_- + 3E_-^2 + E_+ \times E_+ \times E_+ + 3E_+ \times E_- \times E_-) (e^{2i\theta} + e^{-2i\theta}) + \\
& \left. 6(E_+^2 + 8E_+E_- + E_-^2 + 4E_+ \times E_- \times E_-) \right) + \dots \Big] + \\
& \frac{V^3}{3!} \left[m^3 \left(\frac{\Sigma}{2} \right)^3 (e^{3i\theta} + 3e^{i\theta} + 3e^{-i\theta} + e^{-3i\theta}) + \right. \\
& \frac{m^4}{2} \left(\frac{\Sigma}{2} \right)^4 \left(3E_+ (e^{4i\theta} + e^{-4i\theta}) + 6(E_+ + E_-) (e^{2i\theta} + e^{-2i\theta}) + (E_+ + 2E_-) \right) + \dots \Big] + \\
& \frac{V^4}{4!} \left[m^4 \left(\frac{\Sigma}{2} \right)^4 (e^{4i\theta} + 4e^{2i\theta} + 6 + 4e^{-2i\theta} + e^{-4i\theta}) + \dots \right] + \dots \\
& =: \frac{V}{1!} \epsilon + \frac{V^2}{2!} \epsilon^2 + \frac{V^3}{3!} \epsilon^3 + \dots
\end{aligned} \tag{58}$$

This result indicates an exponentiation of the exact vacuum functional, too,

$$\frac{Z(m, \theta)}{Z(0, 0)} = e^{V\epsilon(m, \theta)} \tag{59}$$

where

$$\begin{aligned}
\epsilon(m, \theta) = & m \frac{\Sigma}{2} 2 \cos \theta + \frac{m^2}{2!} \left(\frac{\Sigma}{2} \right)^2 (2E_+ \cos 2\theta + 2E_-) + \\
& \frac{m^3}{3!} \left(\frac{\Sigma}{2} \right)^3 \left((3E_+^2 + E_+ \times E_+ \times E_+) 2 \cos 3\theta + 3(2E_+E_- + E_-^2 + E_+ \times E_- \times E_-) 2 \cos \theta \right) + \dots
\end{aligned} \tag{60}$$

This exponentiation, equ. (59), is, of course, very important, because it guarantees that physical VEVs do not depend on the space-time volume V and are therefore IR-finite. Therefore, it would be nice if equ. (59) could be proven generally. This is indeed possible and shall be discussed next.

For this purpose, let us write $Z(m, \theta)$ as a double sum,

$$Z(m, \theta) = \sum_{l=0}^{\infty} \frac{m^l}{l!} \sum_{n=0}^l V^n c_{l,n}, \tag{61}$$

where the factorial has been introduced as in the perturbation expansion (49).

Because of the multinomial formula

$$(\epsilon(m, \theta))^n = (mc_{1,1} + \frac{m^2}{2!}c_{2,1} + \dots)^n =$$

$$\sum_{l=0}^{\infty} m^{n+l} \sum_{\substack{k_i=0 \\ \sum_i k_i=n, \sum_i i k_i=n+l}}^n \frac{n!}{k_1! \dots k_{n+l}!} \left(\frac{c_{1,1}}{1!}\right)^{k_1} \dots \left(\frac{c_{n+l,1}}{(n+l)!}\right)^{k_{n+l}} \quad (62)$$

the exponentiation condition reads (the $\frac{1}{n!}$ stems from the factor $\frac{V^n}{n!}$)

$$\frac{c_{n+l,n}}{(n+l)!} = \frac{1}{n!} \sum_{\substack{k_i=0 \\ \sum_i k_i=n, \sum_i i k_i=n+l}}^n \frac{n!}{k_1! \dots k_{n+l}!} \left(\frac{c_{1,1}}{1!}\right)^{k_1} \dots \left(\frac{c_{n+l,1}}{(n+l)!}\right)^{k_{n+l}}$$

or

$$c_{n+l,n} = \sum_{\substack{k_i=0 \\ \sum_i k_i=n, \sum_i i k_i=n+l}}^n \frac{(n+l)!}{k_1! \dots k_{n+l}!} \left(\frac{c_{1,1}}{1!}\right)^{k_1} \dots \left(\frac{c_{n+l,1}}{(n+l)!}\right)^{k_{n+l}}. \quad (63)$$

Next we have to answer the question where the volume factors V come from. The first power V stems from the fact that all “propagators” $E_{\pm}(x_i - x_j)$ depend on coordinate *differences*. Higher powers occur when the corresponding “Feynman graph” is disconnected. Let us show a graphical example in Fig. 1.



Fig. 1

Here each wavy line represents a $E_{\pm}(x)$ and their endpoints represent “vertices” $\frac{m\Sigma}{2}e^{\pm i\theta}$. These Feynman rules will be discussed in detail in Section 7.

Obviously, Fig. 1 is of third power in V and of 8th power in m (8 vertices). In general, $c_{l,n}$ is just the sum of all graphs of l -th order that consist of n connected pieces.

Therefore, we just have to prove that (63) is the correct combinatorial formula for the distribution of n connected graphs of total order $n+l$ on $n+l$ vertices.

But this is easy to understand. Consider e.g. a graph $c_{l_1+l_2,2}$ consisting of two connected pieces $c_{l_1,1}$, $c_{l_2,1}$. There are $(l_1+l_2)!$ possibilities to distribute the two connected graphs on l_1+l_2 vertices. However, $l_1!$ ($l_2!$) ways exist to rearrange $c_{l_1,1}$ ($c_{l_2,1}$) on a given subset of l_1 (l_2) vertices, therefore these factors must be divided out. This leads to

$$c_{l_1+l_2,2} = (l_1+l_2)! \frac{c_{l_1,1}}{l_1!} \frac{c_{l_2,1}}{l_2!}$$

and easily may be generalized to explain (63) up to the k_i factors. When some connected subgraphs $c_{i,1}$ occur more than once, $k_i > 1$, there is an additional symmetry factor $\frac{1}{k_i!}$ that counts for the fact that an exchange of identical subgraphs $c_{i,1}$ leads to the same contribution to $c_{n+l,n}$. This explains formula (63).

So we have proven the exponentiation of the vacuum functional, (59) and, as a consequence, the IR-finiteness of the mass perturbation theory. In fact, the expansion of $e^{\pm 4\pi D_{\mu_0}(x)} = (1 + E_{\pm}(x))$ into $E_{\pm}(x)$ is analogous to the cluster expansion of statistical physics models. There, our result correspond to the fact that the free energy is an extensive quantity. A more rigorous discussion of these features can be found in [29,30].

Before ending this section we want to give an explicit (numerical) formula for the lowest orders of the vacuum energy density, $\epsilon(m, \theta)$, and, as a consequence, we will meet the problem of UV regularization. For a numerical evaluation of order m^2 we have to compute the coefficients E_+ and E_- . First, both E_+ and E_- are proportional to $\frac{1}{\mu_0^2}$. Scaling μ_0 out, we find

$$\begin{aligned}\mu_0^2 E_+ &= \mu_0^2 \int d^2x E_+(x) = \int d^2x (e^{-2K_0(|x|)} - 1) \\ &= 2\pi \int_0^\infty dr r (e^{-2K_0(r)} - 1) = -8.9139\end{aligned}\quad (64)$$

$E_+(x)$ is well behaving ($E_+(0) = -1$), so the numerical integration is straight forward. $E_-(x)$ is singular at $x = 0$, $E_-(x) \sim \frac{1}{x^2}$ for $x \rightarrow 0$, but this singularity can easily be understood and removed in a unique way. Indeed, this singularity is just the free fermion singularity, as can be seen by rewriting $E_-(x)$ like (see e.g. equ. (41))

$$\left(\frac{\Sigma}{2}\right)^2 (E_-(x) + 1) = \langle S_+(x) S_-(0) \rangle_0 = G_0^2(x) e^{4\pi(\mathbf{G}(0) - \mathbf{G}(x))} \xrightarrow{|x| \rightarrow 0} G_0^2(x) = \frac{1}{4\pi^2 x^2}. \quad (65)$$

This singularity may be isolated by a partial integration:

$$\begin{aligned}\mu_0^2 E_- &= \int d^2x (e^{2K_0(|x|)} - 1) = 2\pi \int_0^\infty \frac{dr}{r} (e^{2K_0(r)+2\ln r} - r^2) \\ &= 2\pi \left[(\ln r) (e^{2K_0(r)+2\ln r} - r^2) \right]_{\epsilon \rightarrow 0}^\infty + \\ &\quad 2\pi \int_0^\infty dr 2(\ln r) \left((K_1(r) - \frac{1}{r}) e^{2K_0(r)+2\ln r} + r \right)\end{aligned}\quad (66)$$

($K_0' = -K_1$). Observe that the first term precisely leads to the free fermionic singularity at the lower boundary (and vanishes at the upper boundary). So the second term is the unique and finite result we are looking for. The numerical integration gives

$$\mu_0^2 E_- = 9.7384 \quad (67)$$

In the literature there exist other UV regularizations as, e.g. the introduction of an additional Thirring-type interaction ([30,33]). Of course, when this Thirring-type coupling constant is set equal to zero at the end of the computations, the result agrees with our regularization.

With the help of (64), (67) the vacuum energy density reads

$$\epsilon(m, \theta) = m\Sigma \cos \theta + \frac{m^2}{\mu_0^2} \left(\frac{\Sigma}{2}\right)^2 (-8.9139 \cos 2\theta + 9.7384) + o(m^3). \quad (68)$$

Higher order contributions to $\epsilon(m, \theta)$ (and to bosonic n -point functions to be discussed in later sections) may contain logarithmic singularities like in (66) and may be regulated in a

similar manner. However, one may perhaps hope for an even better UV behaviour in higher order computations. After all, the model is known to be super-renormalizable (in ordinary electrical coupling perturbation theory this feature is obvious, as the vacuum polarization graph (= a loop of two fermions) is the only divergent diagram). So one might expect cancellations of divergencies in higher order computations. And, indeed, for the $o(m^2)$ contribution to the Schwinger mass precisely this happens (see Section 8, (99)). A more detailed discussion of this problem will be given elsewhere.

VI. CONDENSATES, SUSCEPTIBILITIES AND CONFINEMENT

In this section we will try to extract some physical information from our results obtained so far. The simplest task is the computation of the fermion condensate,

$$\begin{aligned}\langle S(x) \rangle &= \langle \bar{\Psi}(x) \Psi(x) \rangle = \frac{1}{V} \frac{1}{Z(m, \theta)} \frac{\partial}{\partial m} Z(m, \theta) = \frac{\partial}{\partial m} \epsilon(m, \theta) \\ \langle \bar{\Psi}(x) \Psi(x) \rangle &= \Sigma \cos \theta + \frac{m}{2} \Sigma^2 (E_+ \cos 2\theta + E_-) + o(m^2).\end{aligned}\tag{69}$$

Of course, the order zero result is the condensate of the massless Schwinger model. From this result the pseudoscalar VEV $\langle P(x) \rangle$ may be obtained, e.g. by the substitution $\cos n\theta \rightarrow i \sin n\theta$ ($n = 0, 1, \dots$),

$$\langle P(x) \rangle = \langle \bar{\Psi}(x) \gamma_5 \Psi(x) \rangle = i \Sigma \sin \theta + i \frac{m}{2} \Sigma^2 E_+ \sin 2\theta + o(m^2).\tag{70}$$

Another quantity that may be easily obtained is the field strength condensate (see equ. (21))

$$\langle F(x) \rangle = \frac{2\pi}{e} \frac{\partial}{\partial \theta} \epsilon(m, \theta) = -\frac{2\pi}{e} m \Sigma \sin \theta - \frac{\pi}{e} m^2 \Sigma^2 E_+ \sin 2\theta + o(m^3).\tag{71}$$

Therefore, as discussed in Section 2, whenever there is a classical background field, $F \sim \theta$, there remains some effect on the quantum level and the screening is not complete in the massive model.

Observe that there is a relation between $\langle P \rangle$ and $\langle F \rangle$. This is due to the anomaly equation (11),

$$0 = \partial_\mu \langle J_5^\mu \rangle = \frac{e}{\pi} \langle F \rangle - 2im \langle P \rangle\tag{72}$$

(one-point functions are always constants because of translational invariance).

By performing a second derivative on $\epsilon(m, \theta)$ one may infer the susceptibilities. For the scalar susceptibility we get

$$\chi_s = \int dx \langle S(x) S(0) \rangle_c = \frac{\partial^2}{\partial m^2} \epsilon(m, \theta) = \frac{1}{2} \Sigma^2 (E_+ \cos 2\theta + E_-) + o(m)\tag{73}$$

(the subscript c indicates the connected component; our discussion of the last section explains why only connected components may contribute to $\epsilon(m, \theta)$). For the pseudo-scalar susceptibility the mixed contractions S_+ , S_- get a minus sign,

$$\chi_p = \int dx \langle P(x)P(0) \rangle_c = \frac{1}{2} \Sigma^2 (E_+ \cos 2\theta - E_-) + o(m). \quad (74)$$

The topological susceptibility is

$$\begin{aligned} \chi_{\text{top}} &= \left(\frac{-ie}{2\pi} \right)^2 \int dx \langle F(x)F(0) \rangle_c = -\frac{\partial^2}{\partial \theta^2} \epsilon(m, \theta) = \\ &= m\Sigma \cos \theta + m^2 \Sigma^2 E_+ \cos 2\theta + o(m^3). \end{aligned} \quad (75)$$

There is a relation between χ_p and χ_{top} ; however, this and related questions will be discussed in a later section, where the Dyson-Schwinger equations corresponding to the equations of motion (10), (11) are derived. More on the physical meaning of susceptibilities in two-dimensional models may be found e.g. in [43].

A further physical feature that we are able to discuss by using our results obtained so far is the confinement behaviour of the massive Schwinger model. This was recently discussed in [44] in first order mass perturbation, and we follow their approach and generalize their result to arbitrary order.

A usual way to derive the confinement property is the computation of the string tension from the Wilson loop. The Wilson loop for a test particle of arbitrary charge $g = qe$ is defined as (the additional factor i in Stokes' law is due to our Euclidean conventions (imaginary F), see e.g. [19,17])

$$W_D = \langle e^{ig \int_{\partial D} A_\mu dx^\mu} \rangle = \langle e^{g \int_D F(x) d^2x} \rangle = \langle e^{2\pi i q \int_D \nu(x) d^2x} \rangle \quad (76)$$

where $\nu(x)$ is the Pontryagin index density. Further ∂D is the contour of a closed loop and D the enclosed region of space-time. We are interested in the string tension for very large distances; further we are able to explicitly separate the area dependence, therefore we may set $D \rightarrow V$ in the sequel.

For the VEV of an exponential the following formula holds,

$$\langle e^{2\pi i q \nu} \rangle = \exp \left[\sum_{n=1}^{\infty} \frac{(2\pi i q)^n}{n!} \langle \nu^n \rangle_c \right] \quad (77)$$

where $\langle \rangle_c$ denotes the connected part of the n -point function. These VEVs are given by

$$\langle \nu^n \rangle_c = V \int dx_2 \dots dx_n \langle \nu(0) \nu(x_2) \dots \nu(x_n) \rangle_c = V (-i)^n \frac{\partial^n}{\partial \theta^n} \epsilon(m, \theta) \quad (78)$$

as is obvious from the vacuum functional (21) (as usual, disconnected VEVs are of higher order in V). The vacuum energy density of arbitrary order may be written like

$$\epsilon(m, \theta) = \sum_{l=0}^{\infty} \epsilon_l \cos l\theta \quad (79)$$

where we used the symmetry of $\epsilon(m, \theta)$ with respect to positive and negative instanton number, and ϵ_l acquires contributions from instanton sectors $k = \pm l$. Performing the derivatives (78) we have to separate even ($\sim \cos l\theta$) and odd ($\sim \sin l\theta$) powers of derivatives. We find for the Wilson loop

$$\begin{aligned}
W &= \exp \left[V \sum_{n=1}^{\infty} \frac{(2\pi q)^{2n}}{(2n)!} \sum_{l=0}^{\infty} (-1)^n l^{2n} \epsilon_l \cos l\theta + V \sum_{n=1}^{\infty} \frac{(2\pi q)^{2n-1}}{(2n-1)!} \sum_{l=0}^{\infty} (-1)^n l^{2n-1} \epsilon_l \sin l\theta \right] \\
&= \exp \left[V \sum_{l=0}^{\infty} \epsilon_l \cos l\theta \sum_{n=1}^{\infty} (-1)^n \frac{(2\pi ql)^{2n}}{(2n)!} + V \sum_{l=1}^{\infty} \epsilon_l \sin l\theta \sum_{n=1}^{\infty} (-1)^n \frac{(2\pi ql)^{2n-1}}{(2n-1)!} \right] \\
&= \exp \left[V \sum_{l=0}^{\infty} \epsilon_l \cos l\theta (\cos 2\pi ql - 1) - V \sum_{l=0}^{\infty} \epsilon_l \sin l\theta \sin 2\pi ql \right]. \tag{80}
\end{aligned}$$

The string tension is defined as

$$\sigma := -\frac{1}{V} \ln W = \sum_{l=0}^{\infty} \epsilon_l \left(\cos l\theta (1 - \cos 2\pi ql) + \sin l\theta \sin 2\pi ql \right) \tag{81}$$

and may be interpreted as the force between two widely separated probe charges $g = qe$, where all quantum effects are included.

We find that, whenever the probe charge is an *integer* multiple of the fundamental charge, $q \in \mathbf{N}$, the charges are screened, and the Wilson loop does not obey an area law. Observe that this result is *exact* !

For noninteger probe charges there is no complete screening and the string tension may be computed perturbatively,

$$\sigma = m\Sigma \left(\cos \theta (1 - \cos 2\pi q) + \sin \theta \sin 2\pi q \right) + o(m^2) \tag{82}$$

showing that in the massive Schwinger model and for noninteger probe charges there remains a constant force (linearly rising potential) for very large distances. So in the massive Schwinger model true confinement is realized instead of charge screening in the general case. Observe that this formation of a long range force is a strictly nonperturbative phenomenon in the sense of conventional perturbation theory, because only nontrivial instanton sectors ($k \neq 0$) contribute to the string tension, as is obvious from (78).

On the other hand, in the massless model arbitrary probe charges are screened. (Discussions of screening and confinement in the massive Schwinger model within other approaches may be found e.g. in [11,24,38,40,45], and the behaviour found there agrees with our result.)

VII. FEYNMAN RULES FOR MASS PERTURBATION THEORY

The interaction Lagrangian for the mass perturbation expansion reads $L_I = m\bar{\Psi}\Psi$, see (49). On the other hand, the formulae (44), (48) for VEVs of the massless model, that we need for the perturbation expansion, contain chiral currents S_{\pm} instead of the scalar one in L_I . As a consequence, each vertex corresponding to L_I contains in fact two vertices,

$$m\langle S(x) \rangle_0 = m\langle S_+(x) \rangle_0 + m\langle S_-(x) \rangle_0 = \frac{m\Sigma}{2} e^{i\theta} + \frac{m\Sigma}{2} e^{-i\theta} \tag{83}$$

corresponding to the two chiralities.

Further, these two types of vertices are connected by two types of propagators, namely $S_+(x)S_+(y)$ and $S_-(x)S_-(y)$ by $E_+(x-y)$, and $S_+(x)S_-(y)$ and $S_-(x)S_+(y)$ by $E_-(x-y)$. Further, because all vertices may be connected to each other (see (44)), up to $n-1$

lines $E_{\pm}(x - y_i)$ may run from one vertex x to the other vertices y_i for a n -th order mass perturbation contribution.

As a consequence, the Feynman rules acquire a matrix structure. More precisely, the propagator corresponding to the $E_{\pm}(x)$ is a matrix, which in momentum space reads

$$\mathcal{E}(p) = \begin{pmatrix} \tilde{E}_+(p) & \tilde{E}_-(p) \\ \tilde{E}_-(p) & \tilde{E}_+(p) \end{pmatrix} \quad (84)$$

where the individual entries correspond to the individual $\langle S_i(x)S_j(y) \rangle_0$, $i, j = \pm$, propagators.

Each vertex, where n propagator lines $\mathcal{E}(p_i)$ meet, is a n -th rank tensor \mathcal{G}_0 . Only two components of this tensor are nonzero, namely

$$\mathcal{G}_{0++++} = \frac{m\Sigma}{2}e^{i\theta} \quad , \quad \mathcal{G}_{0-----} = \frac{m\Sigma}{2}e^{-i\theta} \quad (85)$$

(corresponding to $S = S_+ + S_-$). E.g. the vertex where two propagators meet is a matrix

$$\mathcal{G}_0 = \begin{pmatrix} \frac{m\Sigma}{2}e^{i\theta} & 0 \\ 0 & \frac{m\Sigma}{2}e^{-i\theta} \end{pmatrix}. \quad (86)$$

Internal lines must be $\mathcal{E}(p)$ propagators; external lines, however, may be boson lines, too, when we treat bosonic n -point functions $\langle i\Phi(x_1) \dots i\Phi(x_n) \rangle_m$. In (48) we see that each boson that is connected to a S_- vertex acquires a minus sign. Therefore, the rule for a boson line is that each vertex $S = S_+ + S_-$, where a boson line meets, is multiplied by $2\sqrt{\pi}$ times the boson propagator $\frac{-1}{p^2 + \mu_0^2}$ times the pseudoscalar vector P , where

$$P = \begin{pmatrix} 1 \\ -1 \end{pmatrix} \quad , \quad S = \begin{pmatrix} 1 \\ 1 \end{pmatrix}. \quad (87)$$

When n bosons meet at one vertex, one may, instead of contracting that vertex with n vectors P , contract it with one P (S) if n is odd (even). Of course, the number of indices of the vertex must be reduced accordingly.

These Feynman rules may be given by the graphs of Fig. 2 (we display them in momentum space).

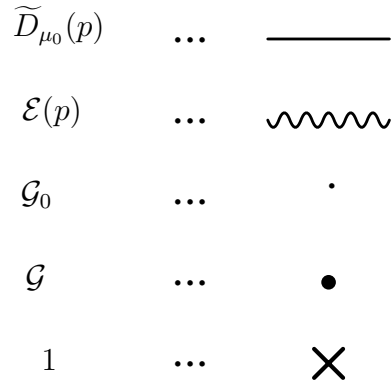


Fig. 2

Here \mathcal{G} denotes the renormalized coupling that may be found like follows. The bare couplings are $m\langle S_{\pm} \rangle_0 = \frac{m\Sigma}{2}e^{\pm i\theta}$, therefore the renormalized couplings are defined as

$$g_\theta = m\langle S_+(x)\rangle_m \quad , \quad g_\theta^* = m\langle S_-(x)\rangle_m \quad (88)$$

and \mathcal{G} is constructed out of g_θ, g_θ^* like \mathcal{G}_0 out of $\frac{m\Sigma}{2}e^{\pm i\theta}$, see (85). Graphically, \mathcal{G} is just the sum of all graphs that may be attached to the bare vertex \mathcal{G}_0 , see Fig. 3,

$$\bullet = \cdot + \text{self-energy loop} + \text{tadpole} + \text{higher order} + \dots$$

Fig. 3

i.e. the sum of all graphs where a line of propagators either starts and ends at the same point, or it ends in the vacuum with zero momentum. g_θ may be easily computed to be

$$\begin{aligned} g_\theta &= \frac{m\Sigma}{2}e^{i\theta} + \left(\frac{m\Sigma}{2}\right)^2(e^{2i\theta}E_+ + E_-) + o(m^3) \\ &=: g_1 + g_2 + o(m^3) \end{aligned} \quad (89)$$

In fact, because of $g_\theta = m\langle S_+\rangle_m$, it is related to the vacuum energy density, see (69),

$$g_\theta + g_\theta^* = m\frac{\partial}{\partial m}\epsilon(m, \theta). \quad (90)$$

Further, because each vertex may be connected to all the other vertices in our theory, the contributions to the renormalized coupling, Fig. 3, may be attached to each vertex of an arbitrary graph and, therefore, all the vertices of the theory may be renormalized from \mathcal{G}_0 to \mathcal{G} .

As a further example of these Feynman rules we will investigate the bosonic two-point function in the next section (we will compute it explicitly there). In addition, we will use these Feynman rules extensively in Sections 9 – 11.

VIII. THE SCHWINGER MASS

As usual, in order to compute VEVs for the massive Schwinger model one has to insert the corresponding operators into the path integral (20) and divide by the vacuum functional $Z(m, \theta)$ (see (59), (60)),

$$\langle \hat{O} \rangle_m = \frac{1}{Z(m, \theta)} \langle \hat{O} \sum_{n=0}^{\infty} \frac{m^n}{n!} \prod_{i=1}^n \int dx_i \bar{\Psi}(x_i) \Psi(x_i) \rangle_0 \quad (91)$$

We will find that via the normalization all volume factors cancel completely, as it certainly has to be.

The Schwinger mass may be inferred from the Schwinger-boson two-point function. Therefore, as a starting point for the mass perturbation computation we need the following n -point functions of the massless model,

$$\langle i\Phi(y_2)i\Phi(y_1) \prod_{i=1}^n S_{H_i}(x_i) \rangle_0 = e^{ik\theta} \left(\frac{\Sigma}{2}\right)^n e^{4\pi \sum_{k<l} \sigma_k \sigma_l D_{\mu 0}(x_k - x_l)}.$$

$$\cdot \left[D_{\mu_0}(y_1 - y_2) + 4\pi \left(\sum_{i=1}^n (-)^{\sigma_i} D_{\mu_0}(x_i - y_2) \right) \left(\sum_{j=1}^n (-)^{\sigma_j} D_{\mu_0}(x_j - y_1) \right) \right] \quad (92)$$

$$k = \sum_{i=1}^n \sigma_i$$

which may be easily computed from the generating functionals (48).

For a perturbative computation of the Schwinger boson propagator we simply have to insert successive orders of (92) into the perturbation formula (91). Doing so, we find up to second order

$$\begin{aligned} \langle i\Phi(y_1)i\Phi(y_2) \rangle_m &= \frac{1}{Z(m, \theta)} \left[D_{\mu_0}(y_1 - y_2) + m \frac{\Sigma}{2} (e^{i\theta} + e^{-i\theta}) V D_{\mu_0}(y_1 - y_2) + \right. \\ &\quad \left. 4\pi m \frac{\Sigma}{2} (e^{i\theta} + e^{-i\theta}) \int dx D_{\mu_0}(x - y_1) D_{\mu_0}(x - y_2) + \right. \\ &\quad \left. \frac{m^2}{2!} \left(\frac{\Sigma}{2} \right)^2 (e^{2i\theta} + e^{-2i\theta}) \int dx_1 dx_2 [D_{\mu_0}(y_1 - y_2) + 4\pi (D_{\mu_0}(x_1 - y_1) + D_{\mu_0}(x_2 - y_1)) \cdot \right. \\ &\quad \left. \cdot (D_{\mu_0}(x_1 - y_2) + D_{\mu_0}(x_2 - y_2))] e^{4\pi D_{\mu_0}(x_1 - x_2)} + \right. \\ &\quad \left. \frac{m^2}{2!} \left(\frac{\Sigma}{2} \right)^2 2 \int dx_1 dx_2 [D_{\mu_0}(y_1 - y_2) + 4\pi (D_{\mu_0}(x_1 - y_1) - D_{\mu_0}(x_2 - y_1)) \cdot \right. \\ &\quad \left. \cdot (D_{\mu_0}(x_1 - y_2) - D_{\mu_0}(x_2 - y_2))] e^{-4\pi D_{\mu_0}(x_1 - x_2)} \right]. \quad (93) \end{aligned}$$

Inserting $Z(m, \theta)$ up to second order (see (59), (60)) and expanding the denominator in the usual perturbative fashion, we arrive at

$$\begin{aligned} \langle i\Phi(y_1)i\Phi(y_2) \rangle_m &= D_{\mu_0}(y_1 - y_2) + 4\pi m \Sigma \cos \theta \int dx D_{\mu_0}(x - y_1) D_{\mu_0}(x - y_2) + \\ &\quad 4\pi m^2 \left(\frac{\Sigma}{2} \right)^2 \cos 2\theta \int dx_1 dx_2 [2D_{\mu_0}(x_1 - y_1) D_{\mu_0}(x_1 - y_2) + 2D_{\mu_0}(x_1 - y_1) D_{\mu_0}(x_2 - y_2)] \cdot \\ &\quad \cdot (E_+(x_1 - x_2) + 1) - 8\pi m^2 \left(\frac{\Sigma}{2} \right)^2 \cos 2\theta V \int dx D_{\mu_0}(x - y_1) D_{\mu_0}(x - y_2) + \\ &\quad 4\pi m^2 \left(\frac{\Sigma}{2} \right)^2 \int dx_1 dx_2 [2D_{\mu_0}(x_1 - y_1) D_{\mu_0}(x_1 - y_2) - 2D_{\mu_0}(x_1 - y_1) D_{\mu_0}(x_2 - y_2)] \cdot \\ &\quad \cdot (E_-(x_1 - x_2) + 1) - 8\pi m^2 \left(\frac{\Sigma}{2} \right)^2 V \int dx D_{\mu_0}(x - y_1) D_{\mu_0}(x - y_2) \end{aligned}$$

$$\begin{aligned}
&= D_{\mu_0}(y_1 - y_2) + 4\pi m \frac{\Sigma}{2} \cos \theta \int dx D_{\mu_0}(x - y_1) D_{\mu_0}(x - y_2) + \\
&8\pi m^2 \left(\frac{\Sigma}{2}\right)^2 \int dx_1 dx_2 D_{\mu_0}(x_1 - y_1) D_{\mu_0}(x_2 - y_2) [\cos 2\theta E_+(x_1 - x_2) - E_-(x_1 - x_2)] + \\
&8\pi m^2 \left(\frac{\Sigma}{2}\right)^2 (\cos 2\theta E_+ + E_-) \int dx D_{\mu_0}(x - y_1) D_{\mu_0}(x - y_2) + \\
&8\pi m^2 \left(\frac{\Sigma}{2}\right)^2 (\cos 2\theta - 1) \int dx_1 dx_2 D_{\mu_0}(x_1 - y_1) D_{\mu_0}(x_2 - y_2) \tag{94}
\end{aligned}$$

where $E_{\pm}, E_{\pm}(x)$ are given in (52) and we used the $x \rightarrow -x$ symmetry of all occurring functions. The last term stems from a disconnected part of (93) and must be subtracted. Observe that, as claimed, all volume factors V have dropped out.

We may easily check that (94) is the right expression by depicting the corresponding Feynman diagrams in Fig. 4

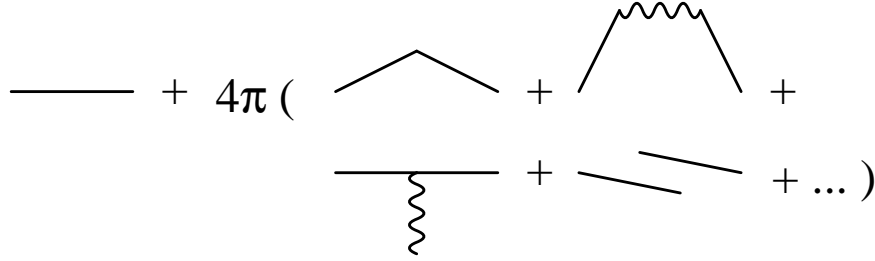


Fig. 4

and find that (94) and Fig. 4 coincide. Again, the last graph is disconnected and must be subtracted.

In order to obtain the second order result for the Schwinger mass, we rewrite expression (94) in momentum space and substitute all functions by their Fourier transforms (thereby the convolutions turn into products; the disconnected term in (94) is omitted),

$$\begin{aligned}
\langle i\widetilde{\Phi}i\Phi \rangle_m^c(p) &= \frac{-1}{p^2 + \mu_0^2} + 4\pi m \Sigma \cos \theta \frac{1}{(p^2 + \mu_0^2)^2} + \\
2\pi m^2 \Sigma^2 \frac{1}{(p^2 + \mu_0^2)^2} &[\cos 2\theta (E_+ + \tilde{E}_+(p)) + E_- - \tilde{E}_-(p)] = \\
\frac{-1}{p^2 + \mu_0^2} &\left(1 - 4\pi m \Sigma \cos \theta \frac{1}{p^2 + \mu_0^2} - 2\pi m^2 \Sigma^2 [\cos 2\theta (E_+ + \tilde{E}_+(p)) + E_- - \tilde{E}_-(p)] \frac{1}{p^2 + \mu_0^2}\right) = \\
\frac{-1}{p^2 + \mu_0^2 + 4\pi m \Sigma \cos \theta + 2\pi m^2 \Sigma^2 [\cos 2\theta (E_+ + \tilde{E}_+(p)) + E_- - \tilde{E}_-(p)] + (4\pi m \Sigma \cos \theta)^2 \frac{1}{p^2 + \mu_0^2}} &
\end{aligned}$$

$$+ o(m^3) \quad (95)$$

Therefore, for finding the mass pole, p^2 has to obey the equation (after a rescaling $p'^2 = \frac{p^2}{\mu_0^2}$, $E'_\pm = E_\pm(\mu_0^2 \equiv 1) = \mu_0^2 E_\pm$ etc.)

$$\begin{aligned} p'^2 = -1 - 4\pi \frac{m\Sigma}{\mu_0^2} \cos \theta - 2\pi \frac{m^2 \Sigma^2}{\mu_0^4} \cos 2\theta [E'_+ + \tilde{E}'_+(p') + \frac{4\pi}{p'^2 + 1}] - \\ 2\pi \frac{m^2 \Sigma^2}{\mu_0^4} [E'_- - \tilde{E}'_-(p') + \frac{4\pi}{p'^2 + 1}]. \end{aligned} \quad (96)$$

The second order part (the term in square brackets) may be further evaluated like (for the $\cos 2\theta$ term)

$$\begin{aligned} [\dots] = \int d^2x [e^{-2K_0(|x|)} - 1 + e^{ip'x}(e^{-2K_0(|x|)} - 1 + 2K_0(|x|))] = \\ \int_0^\infty dr r [2\pi(e^{-2K_0(r)} - 1) + \int_0^{2\pi} d\theta e^{ip'|r \cos \theta} (e^{-2K_0(r)} - 1 + 2K_0(r))] = \\ 2\pi \int_0^\infty dr r [e^{-2K_0(r)} - 1 + J_0(|p'|r)(e^{-2K_0(r)} - 1 + 2K_0(r))] \end{aligned} \quad (97)$$

where J_0 is the Bessel function of the first kind. This expression behaves well around $|p'| = i$ and therefore we may set $|p'| = i$ because deviations from this value are of higher order in m . Using $I_0(r) = J_0(ir)$ we find

$$\frac{1}{2\pi} [\dots] =: A = \int_0^\infty dr r [e^{-2K_0(r)} - 1 + I_0(r)(e^{-2K_0(r)} - 1 + 2K_0(r))] = -0.6599 \quad (98)$$

Analogously we find for the other second order term (containing the E_-)

$$\frac{1}{2\pi} [\dots] =: B = \int_0^\infty dr r [e^{+2K_0(r)} - 1 + I_0(r)(-e^{+2K_0(r)} + 1 + 2K_0(r))] = 1.7277 \quad (99)$$

In this expression (99) the nice feature of cancellation of UV divergencies occurs. Indeed, both $e^{2K_0(r)}$ and $I_0(r)e^{2K_0(r)}$ diverge like $\frac{1}{r^2}$ for small r (this divergency corresponds to the free fermion field divergency of the underlying theory that we discussed in Section 5, see (65)), but obviously the divergencies cancel each other. In fact, this cancellation was already observed twenty years ago in [16] within a bosonization approach.

Collecting all results we find for the Schwinger mass in second order

$$-p'^2 \equiv \frac{\mu_2^2}{\mu_0^2} = 1 + 4\pi \frac{m}{\mu_0} \frac{\Sigma}{\mu_0} \cos \theta + 4\pi^2 \frac{m^2}{\mu_0^2} \left(\frac{\Sigma}{\mu_0}\right)^2 (A \cos 2\theta + B) \quad (100)$$

or, inserting all numbers (remember $\frac{\Sigma}{\mu_0} = \frac{e^\gamma}{2\pi}$, equ. (40))

$$\mu_2^2 = \mu_0^2 \left(1 + 3.5621 \cdot \frac{m}{\mu_0} \cos \theta + 5.4807 \cdot \frac{m^2}{\mu_0^2} - 2.0933 \cdot \frac{m^2}{\mu_0^2} \cos 2\theta\right). \quad (101)$$

For the special case $\theta = 0$ our result (101) precisely coincides with the result in [46], where the second order correction for $\theta = 0$ was computed within bosonization and using near light cone coordinates. In the same article this result was compared to a lattice calculation ([52]), and a good agreement is obtained within the range of the expansion parameter $\frac{m}{\mu_0}$ where the lattice calculations were performed.

IX. DYSON-SCHWINGER EQUATIONS AND EXACT N -POINT FUNCTIONS

The Schwinger boson – which we discussed in the last section – is an interacting particle in the massive Schwinger model. As a consequence, we will find that it forms n -boson bound states. In principle, their masses could be computed analogously to the previous section, by a computation of the corresponding Schwinger-boson $2n$ -point functions and by the determination of their mass poles.

Here we will adapt a slightly different method. We will discuss the Dyson-Schwinger equations that follow from the equations of motion (10), (11), acquiring thereby a deeper insight into the structure of the model. With the help of these Dyson-Schwinger equations we will be able to re-express the n -point functions of the model in a way that is more suitable for our discussion. We will find in this way that the spectrum of the theory is even richer than expected. There is a second stable particle in the theory in addition to the Schwinger boson, namely the two-boson bound state, and unstable higher bound states may be formed out of both these stable particles. Further, we will find that both particles may occur in final states of decays and scattering processes (see also [62–64]).

When we use the generating functional for Schwinger bosons (48) for a computation of the Schwinger boson $2n$ -point function in lowest order in m , we find a contribution that may be depicted graphically like in Fig. 5,

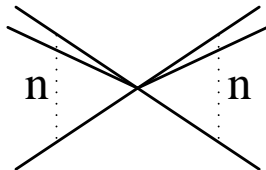


Fig. 5

and the vertex corresponds to a coupling constant c , where

$$c = (4\pi)^n m \Sigma \cos \theta. \quad (102)$$

Therefore, this lowest order coupling mediates an attractive force for $|\theta| < \frac{\pi}{2}$, and in this range of the vacuum angle θ the formation of bound states has to be expected, at least for sufficiently small fermion mass m . The restriction $|\theta| < \frac{\pi}{2}$ shall be assumed in the sequel.

In the introduction we wrote down the two equations of motion that relate the field strength operator and the fermionic vector current operator, namely the Maxwell equation (10) and the anomaly equation (11). By introducing the Schwinger boson (9) and by eliminating the field strength we may derive the equation (expressed in real fields $P, i\Phi$)

$$M_x i\Phi(x) := (\square_x - \mu_0^2) i\Phi(x) = 2\sqrt{\pi} m P(x). \quad (103)$$

(where we introduced the operator M_x for convenience).

[*Remark:* there is a slight difference between the equations (10), (103) and equation (11). Whereas the anomaly equation (11) holds as an operator relation, and consequently on all states, (10) and (103) are only true on physical states (i.e. on states that are invariant with respect to small *and large* gauge transformations; for a deeper discussion of this feature see e.g. [2,11]). However, the introduction of the θ vacuum within our path integral approach precisely corresponds to the introduction of the physical vacuum (see Section 2). Therefore,

for our physical VEVs we may use equ. (103), as we will verify by explicit perturbative computations.]

Next we define the amputated, connected bosonic n -point functions (FT... Fourier transform)

$$M^{(n)}(p_1, \dots, p_n) = \text{FT}(M_{x_1} \dots M_{x_n} \langle i\Phi(x_1) \dots i\Phi(x_n) \rangle_m^c). \quad (104)$$

A. Two-point function

So let us study e.g. the connected two-point function $\langle i\Phi(x_1)i\Phi(x_2) \rangle_m^c$. Graphically it may be depicted like in Fig. 6.

$$\text{---} \bigcirc \text{---} = \text{---} + 4\pi \left(\text{triangle loop} + \text{self-energy loop} + \text{self-energy loop} + \text{bubble} + \text{sunset} + \dots \right)$$

Fig. 6

We find the following behaviour: all graphs where both boson lines meet at one and the same vertex contain just the corrections that change this vertex from the bare one \mathcal{G}_0 to the exact (renormalized) vertex \mathcal{G} , see Fig. 3. In all the other graphs, each individual vertex is renormalized in the same way, too.

So let us re-express Fig. 6 in terms of the renormalized coupling, and, in addition, amputate the two external boson lines (and the pseudoscalar vectors P , see (87)). We obtain Fig. 7, where we introduced the exact propagator that is defined in Fig. 8.

$$\text{---} \bigcirc \text{---} = \text{---} \text{---} + 4\pi \text{---} \bigcirc \text{---}$$

Fig. 7

$$\text{---} \bigcirc \text{---} = \bullet + \bullet \text{---} \bullet + \bullet \text{---} \bullet \text{---} \bullet + \text{triangle loop with dots} + \dots$$

Fig. 8

Here it is understood that the left and right vertices of each graph in Fig. 8 are the initial and final ones where we amputated the bosons. We introduce for the above exact propagator of Fig. 8 the name $\mathcal{G}\Pi(p)$ in momentum space (matrix multiplication is understood, see the Feynman rules of Fig. 2), because we will need it frequently

$$\mathcal{G}\Pi(p) := \mathcal{G} + \mathcal{G}\mathcal{E}(p)\mathcal{G} + \mathcal{G}\mathcal{E}(p)\mathcal{G}\mathcal{E}(p)\mathcal{G} + \dots \quad (105)$$

This exact propagator $\Pi(p)$ consists of a constant part (the sole vertex in Fig. 8 without $\mathcal{E}(p)$ lines) that is a scalar (because two boson lines meet on this one vertex), and of a true two-point function (depending on p), where the initial and final vertices are pseudoscalars. Inserting all factors properly, Fig. 7 may be written like ($M^{(2)}(p, p) \equiv M^{(2)}(p)$)

$$M^{(2)}(p) = -(p^2 + \mu_0^2) + 4\pi m \langle S \rangle_m + 4\pi m^2 \langle \widetilde{PP} \rangle_m^c(p) \quad (106)$$

where

$$m \langle S \rangle_m \equiv P^T \mathcal{G} P = S_i \mathcal{G}_i = g_\theta + g_\theta^* \quad (107)$$

$$m^2 \langle \widetilde{PP} \rangle_m^c(p) \equiv P^T \mathcal{G} (\Pi(p) - \mathbf{1}) P \quad (108)$$

where $P^T = (1, -1)$ is the transpose of the vector P , (87), and matrix multiplication is understood (the single vertex \mathcal{G} we may interpret either as a two-component object that is contracted by two vectors P or as a one-component object that is contracted by one vector S).

This is just the momentum space version of the Dyson-Schwinger equation for the two-point function,

$$\begin{aligned} M_{y_1} M_{y_2} \langle i\Phi(y_1) i\Phi(y_2) \rangle &= M_{y_1} \delta(y_1 - y_2) + \\ &4\pi m \langle S(y_1) \rangle_m \delta(y_1 - y_2) + 4\pi m^2 \langle P(y_1) P(y_2) \rangle_m^c. \end{aligned} \quad (109)$$

Observe that the $\langle P(y_1) P(y_2) \rangle$ propagator includes an arbitrary number of bosons propagating from y_1 to y_2 , even in least order. This will be important in the sequel.

The key observation for the computation of bound states is the fact that the exact propagator $\Pi(p)$ may be resummed. This resummation relies on the following observation. All diagrams that fall into two pieces when they are cut at a vertex, factorize in momentum space, i.e. they are a product of two functions of p , see Fig. 8. The opposite type graphs are called non-factorizable (n.f.).

Here we should be more precise about the cutting. We stated in Section 7 that the vertices are tensors, so how to cut such a vertex? Suppose e.g. we have a vertex where three lines meet and we want to cut it in a way that two wavy lines belong to the left hand side, and one line to the right hand side. Then we rewrite the vertex like

$$\mathcal{G}_{ijk} = \delta_{ijl} \mathcal{G}_{ll'k} \delta_{l'l} \quad , \quad i, j, k, l, l' = \pm \quad (110)$$

where $\mathcal{G}_{ll'}$ is the vertex matrix (85,88) and the $\delta_{i_1 \dots i_n}$ are generalizations of the Kronecker delta δ_{ij} , i.e.

$$\delta_{++ \dots +} = \delta_{-- \dots -} = 1 \quad , \quad \delta_{i_1 \dots i_n} = 0 \quad \text{otherwise} \quad (111)$$

Therefore, we may write for the sum of non-factorizable graphs, which we call \mathcal{A} (see Fig. 9)

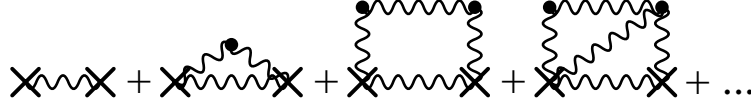


Fig. 9

$$\mathcal{A}_{ij}(p) = \mathcal{E}_{ij}(p) + \int \frac{d^2q}{(2\pi)^2} \delta_{ikk'} \mathcal{E}_{kl}(q) \mathcal{G}_{ll'} \mathcal{E}_{l'm}(q) \mathcal{E}_{k'm'}(q-p) \delta_{jmm'} + \dots \quad (112)$$

The matrix $\mathcal{A}(p)$ may be rewritten like

$$\mathcal{A}(p) = \begin{pmatrix} \langle \widetilde{S_+ S_+} \rangle_{\text{n.f.}}(p) & \langle \widetilde{S_+ S_-} \rangle_{\text{n.f.}}(p) \\ \langle \widetilde{S_- S_+} \rangle_{\text{n.f.}}(p) & \langle \widetilde{S_- S_-} \rangle_{\text{n.f.}}(p) \end{pmatrix} \quad (113)$$

The entries of this matrix are, however, related (e.g. $\langle \widetilde{S_- S_-} \rangle_{\text{n.f.}}(g_\theta, p) = \langle \widetilde{S_+ S_+} \rangle_{\text{n.f.}}(g_\theta^*, p)$, as may be checked from the perturbative expansion) and, therefore, we find for the product $\mathcal{G}\mathcal{A}(p)$ (which we need in the sequel)

$$\mathcal{G}\mathcal{A}(p) =: \begin{pmatrix} \alpha(g_\theta, p) & \beta(g_\theta, p) \\ \beta(g_\theta^*, p) & \alpha(g_\theta^*, p) \end{pmatrix} \quad (114)$$

$$\alpha(g_\theta, p) = g_\theta \langle \widetilde{S_+ S_+} \rangle_{\text{n.f.}}(g_\theta, p) \quad , \quad \beta(g_\theta, p) = g_\theta \langle \widetilde{S_+ S_-} \rangle_{\text{n.f.}}(g_\theta, p). \quad (115)$$

Now we may collect all n.f. graphs in (105), Fig. 8, e.g. on the left hand side, and find that they are again multiplied by *all* graphs that occur in Fig. 8. Therefore we may write for $\mathcal{G}\Pi(p)$ of equ. (105)

$$\mathcal{G}\Pi(p) = \mathcal{G}(\mathbf{1} + \mathcal{A}(p)\mathcal{G}\Pi(p)). \quad (116)$$

Equation (116) may be solved for $\Pi(p)$ by a matrix inversion and has the solution

$$\Pi(p) = \frac{1}{N(p)} \begin{pmatrix} 1 - \alpha(g_\theta^*, p) & \beta(g_\theta^*, p) \\ \beta(g_\theta, p) & 1 - \alpha(g_\theta, p) \end{pmatrix} \quad (117)$$

where $N(p)$ is the determinant of the matrix that had to be inverted,

$$N(p) = \det(\mathbf{1} - \mathcal{G}\mathcal{A}(p)) = 1 - \alpha(g_\theta, p) - \alpha(g_\theta^*, p) + \alpha(g_\theta, p)\alpha(g_\theta^*, p) - \beta(g_\theta, p)\beta(g_\theta^*, p). \quad (118)$$

We will find that the zeros of the real part of the denominator $N(p)$ will give us all bound-state masses, whereas its imaginary parts at the bound-state masses are related to the decay widths.

B. Higher n -point functions

Dyson-Schwinger equations for higher n -point functions may be derived in a way that is similar to the case of the two-point function. Before showing them we need some more graphical rules (see Fig. 10),

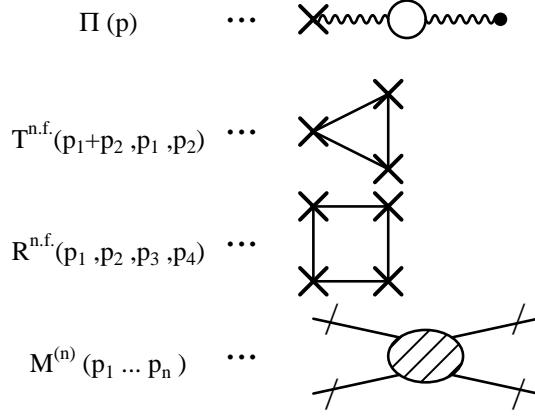


Fig. 10

where $M^{(n)}$, of course, should have n external (amputated) boson lines.

For the three-point function e.g. we find the Dyson-Schwinger equation (in momentum space)

$$M^{(3)}(p_1 + p_2, p_1, p_2) = (2\sqrt{\pi})^3 [m\langle P \rangle_m + m^2\langle \widetilde{SP} \rangle_m^c(p_1 + p_2) + m^2\langle \widetilde{SP} \rangle_m^c(p_1) + m^2\langle \widetilde{SP} \rangle_m^c(p_2) + m^3\langle \widetilde{PPP} \rangle_m^c(p_1 + p_2, p_1, p_2)] \quad (119)$$

where $m\langle P \rangle_m$ and $m^2\langle \widetilde{SP} \rangle_m^c(p)$ are analogous to (107), (108) whereas the last term is given by

$$m^3\langle \widetilde{PPP} \rangle_m^c(p_1 + p_2, p_1, p_2) = P_i P_j P_k \mathcal{G}_{ii'} \mathcal{G}_{jj'} \mathcal{G}_{kk'} T_{i'j'k'}(p_1 + p_2, p_1, p_2) \quad (120)$$

and T_{ijk} is just the exact three-point function for general chiral indices and external couplings equal to 1, see Fig. 11.

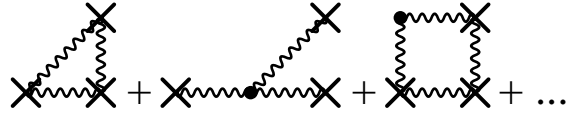


Fig. 11

The essential point is that $M^{(3)}$, again, may be reexpressed entirely in terms of non-factorizable n -point functions, namely

$$M^{(3)}(p_1 + p_2, p_1, p_2) = (2\sqrt{\pi})^3 P_i P_j P_k \Pi_{ii'}(p_1 + p_2) \Pi_{jj'}(p_1) \Pi_{kk'}(p_2) \cdot (\mathcal{G}_{i'j'k'} + \mathcal{G}_{i'l} \mathcal{G}_{j'm} \mathcal{G}_{k'n} T_{lmn}^{n.f.}(p_1 + p_2, p_1, p_2)) \quad (121)$$

or, graphically (see Fig. 12; we ignore an overall factor $(2\sqrt{\pi})^3$ on the r.h.s. of Fig. 12),

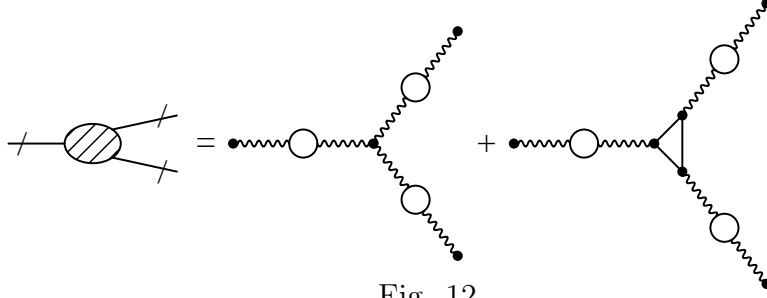


Fig. 12

where the non-factorizable three-point function $T_{\text{n.f.}}$ is given by Fig. 13.

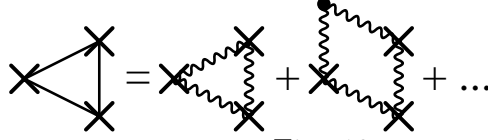


Fig. 13

The actual validity of (121), Fig. 12, has to be checked by a closer inspection of the Feynman graphs (it is just tedious combinatorics).

We find that the non-factorizable n -point functions in our theory play a role analogous to the 1PI Green functions in other theories.

The four-point function $M^{(4)}$ may be treated along similar lines. Again, the Dyson-Schwinger equation allows to express $M^{(4)}$ in terms of $\langle P \dots \rangle_m^c$ and $\langle S \dots \rangle_m^c$ n -point functions (which we show in coordinate space this time),

$$\begin{aligned}
& M_{y_1} M_{y_2} M_{y_3} M_{y_4} \langle \Phi(y_1) \Phi(y_2) \Phi(y_3) \Phi(y_4) \rangle^c = \\
& 16\pi^2 \left[m \langle S(y_1) \rangle \delta(y_1 - y_2) \delta(y_1 - y_3) \delta(y_1 - y_4) + \right. \\
& m^2 \delta(y_1 - y_2) \delta(y_3 - y_4) \langle S(y_1) S(y_3) \rangle^c + \text{perm.} + \\
& m^2 \delta(y_1 - y_2) \delta(y_1 - y_3) \langle P(y_1) P(y_4) \rangle^c + \text{perm.} + \\
& m^3 \delta(y_1 - y_2) \langle S(y_1) P(y_3) P(y_4) \rangle^c + \text{perm.} + \\
& \left. m^4 \langle P(y_1) P(y_2) P(y_3) P(y_4) \rangle^4 \right] \tag{122}
\end{aligned}$$

Further, $M^{(4)}$ may be reexpressed in terms of non-factorizable n -point functions and reads

$$\begin{aligned}
M^{(4)}(p_1, \dots, p_4) = & (4\pi)^2 P_i P_j P_k P_l \Pi_{ii'}(p_1) \Pi_{jj'}(p_2) \Pi_{kk'}(p_3) \Pi_{ll'}(p_4) \left[\mathcal{G}_{i'j'k'l'} \right. \\
& \left. + \mathcal{G}_{i'm} \mathcal{G}_{j'm'} \mathcal{G}_{k'n} \mathcal{G}_{l'n'} R_{mm'nn'}^{\text{n.f.}}(p_1, p_2, p_3, p_4) \right]
\end{aligned}$$

$$\begin{aligned}
& + \left(\mathcal{G}_{i'j'm}(\Pi_{mm'}(p_1 + p_2) - \delta_{mm'})\delta_{m'k'l'} + \text{perm.} \right) \\
& + \left(\mathcal{G}_{i'j'm}\Pi_{mm'}(p_1 + p_2)T_{m'nn'}^{\text{n.f.}}(p_1 + p_2, p_3, p_4)\mathcal{G}_{nk'}\mathcal{G}_{n'l'} + \text{perm.} \right) \\
& + \left(\mathcal{G}_{i'm}\mathcal{G}_{j'm'}T_{mm'n}^{\text{n.f.}}(p_1 + p_2, p_1, p_2)\mathcal{G}_{nn'}\Pi_{n'r}(p_1 + p_2)T_{rr's}^{\text{n.f.}}(p_3 + p_4, p_3, p_4)\mathcal{G}_{r'k'}\mathcal{G}_{sl'} + \text{perm.} \right) \Big] \\
& \hspace{15em} (123)
\end{aligned}$$

where momentum conservation requires $p_1 + p_2 = p_3 + p_4$. Graphically, this identity may be depicted like in Fig. 14 (again we suppress an overall factor $(2\sqrt{\pi})^4$ in Fig. 14).

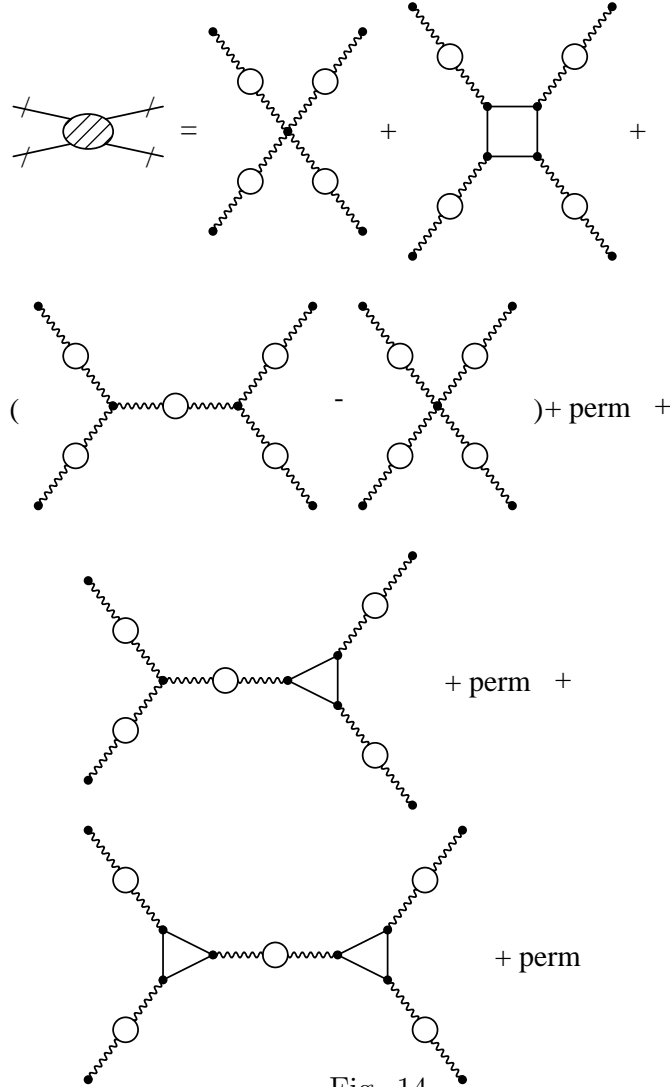


Fig. 14

The permutations in Fig. 14 contain all attachments of the external $\Pi(p_i)$ lines that are topologically distinct (i.e. 3, 6 and 3 permutations).

Observe that in each of the third type diagrams of Fig. 14 the lowest order diagram has to be subtracted in order to avoid an overcounting (this is so because $\Pi(p)$ contains the lowest order, $\mathcal{G}\Pi(p) = \mathcal{G} + o(g_\theta^2)$).

X. BOUND-STATE MASSES AND DECAY WIDTHS

A. General bound-state structure

We claimed at the end of Subsection 9.1 that we could infer all the boson states and decay widths from the two-point function $\Pi(p)$, (117), which we want to discuss now. First, observe that the $\Pi(p)$ propagator also occurs in higher bosonic n -point functions. E.g. for $M^{(4)}$ (Fig. 14), when one takes the third type of diagrams and inserts the lowest order ($\Pi \sim \mathbf{1}$) for the four *external* $\Pi(p_i)$ lines, there remains precisely an internal $\Pi(p_1 + p_2)$ propagator (times \mathcal{G}). Therefore it is not a surprize that we can provide information on higher bosonic states, too, from $\Pi(p)$. In fact, most of the information may be inferred from the denominator $N(p)$, (118), of $\Pi(p)$. The zeros of the real part of $N(p)$ will give all the bound-state masses of the theory – at least the leading order contribution – and the imaginary parts will give the corresponding decay widths ([35,62,63]).

This denominator $N(p)$ reads, in lowest order

$$N(p) = 1 - \alpha(g_\theta, p) - \alpha(g_\theta^*, p) \quad (124)$$

where, again in lowest order

$$\alpha(g_\theta, p) = g_\theta \tilde{E}_+(p) \quad , \quad \beta(g_\theta, p) = g_\theta \tilde{E}_-(p) \quad , \quad g_\theta = m \frac{\Sigma}{2} e^{i\theta} \quad (125)$$

and the $\tilde{E}_\pm(p)$ are the exponentials of bosonic propagators,

$$\tilde{E}_\pm(p) = \sum_{n=1}^{\infty} (\pm 1)^n d_n(p) \quad , \quad d_n(p) := \frac{(4\pi)^n}{n!} \widetilde{D}_{\mu_0}^n(p). \quad (126)$$

The $d_n(p)$ are just n -boson blobs (see Fig. 15 for d_2, d_3)

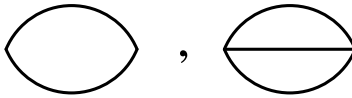


Fig. 15

and have the following properties: at $s = -p^2 = (n\mu)^2$, $d_n(p)$ has a singularity (real particle production threshold), and above this threshold it has an imaginary part. Therefore, slightly below the threshold $(n\mu)^2$, $d_n(p)$ is large enough to balance the coupling constant and make the real part of $N(p)$, (124), vanish,

$$m\Sigma \cos \theta d_n(p) \sim 1 + o(m) \quad (127)$$

and, therefore, causes an n -boson bound state. At the position of the two-boson bound state, $s = M_2^2 = 4\mu^2 - \Delta_2$, $N(p)$ has no imaginary part and, therefore, the two-boson bound state is stable. At the three-boson bound-state mass M_3 , $d_2(s = M_3^2)$ has an imaginary part and, therefore, a decay into two Schwinger bosons (with mass μ) is possible. For higher n -boson bound states the functions d_2, \dots, d_{n-1} have imaginary parts at M_n^2 , therefore decays into $2, \dots, n-1$ Schwinger bosons are possible.

So far this is a lowest order reasoning, but we will find that we have to take into account some higher order effects, too, in order to obtain the physical spectrum of the theory.

One higher-order effect may be understood easily. Remember that the $\alpha(g_\theta, p)$ of (124) stems from the non-factorizable two-point function \mathcal{A} , (114), (in fact, α is the $++$ component of \mathcal{GA}). To get more insight, let us rewrite \mathcal{A} in terms of internal bosons, see Fig. 16.

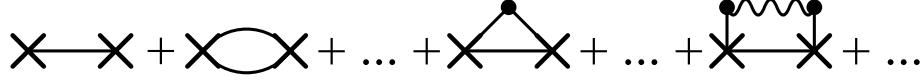


Fig. 16

We find that the one-boson line propagating from the initial to the final external vertex acquires *no* correction, because such corrections would be factorizable and are, therefore, excluded from α . On the other hand, all the higher $d_n(p)$, $n \geq 2$, do get corrections.

This means that for the computation of the lowest pole mass (the Schwinger mass) one needs the bare Schwinger mass as an input, and the renormalized Schwinger mass is provided by the computation. For the higher bound states, on the other hand, one needs the renormalized Schwinger mass as an input in order to compute the bound-state mass poles. The reason is that the mass corrections for the bosons just shift the position of the threshold singularity and are therefore important in lowest order. There are other corrections present, too (internal boson interactions), however, they are unimportant in lowest order.

This result is very plausible physically: the higher bound states should consist of *physical* Schwinger bosons with their physical masses μ (not the bare masses μ_0).

Therefore we redefine the $d_n(p)$ ($n \geq 2$) for the rest of the paper to be

$$d_n(p) := \frac{(4\pi)^n}{n!} \widetilde{D}_\mu^n(p). \quad (128)$$

So we found, up to now, bound states composed of an arbitrary number of Schwinger bosons, where μ and M_2 are stable, and the higher bound states are unstable.

However, this can not yet be the whole story. To understand why, look at the lowest order contribution to the three-point function, Fig. 12, with one incoming $\Pi(p_1)$, one vertex and two outgoing $\Pi(p_2)$, $\Pi(p_3)$. Suppose the incoming $\Pi(p_1)$ is at the mass $-p_1^2 = M_n^2$ of a sufficiently heavy unstable bound state. For a decay into stable final particles all the stable mass poles of $\Pi(p_2)$, $\Pi(p_3)$ are possible. But by our above arguments the mass pole of the stable M_2 particle is present in $\Pi(p_i)$ as well as the mass pole of the Schwinger boson μ . Therefore, Fig. 12 describes decays into M_2 particles as well as μ particles. On the other hand, we did not find imaginary parts (up to now) in $N(p)$ that describe decays into some M_2 , so obviously something is missing.

The M_2 bound state itself was found by a resummation, therefore it is a reasonable idea to use the higher order contributions to α , β for a further resummation. α and β are just components of the non-factorizable propagator $\mathcal{A}(p)$, (114), so let us investigate it more closely.

By a partial resummation we may find the following contribution to $\mathcal{A}(p)$,

$$H_{ii'}(p) := \int \frac{d^2 q}{(2\pi)^2} \delta_{ijk} \mathcal{A}_{jj'}(q) \mathcal{G}_{j'l} \Pi_{ll'}(q) \mathcal{A}_{l'k'}(q) \mathcal{A}_{km}(q-p) \delta_{i'k'm}. \quad (129)$$

This is just a blob where $\mathcal{A}(q-p)$ runs along one line, the other terms run along the other line. We want to discuss the μ - M_2 contribution, therefore we substitute $\mathcal{A}(q-p)$ by its lowest order, one-boson part,

$$\mathcal{A}(q-p) \sim 4\pi \widetilde{D}_\mu(q-p) \begin{pmatrix} 1 & -1 \\ -1 & 1 \end{pmatrix} \quad (130)$$

and the two further $\mathcal{A}(q)$ by their lowest order contribution

$$\mathcal{A}(q) \sim \begin{pmatrix} \widetilde{E}_+(q) & \widetilde{E}_-(q) \\ \widetilde{E}_-(q) & \widetilde{E}_+(q) \end{pmatrix} \quad (131)$$

The resummation that we need in (129) is taken into account by $\Pi(q)$. With these restrictions $H(p)$ corresponds to the graph of Fig. 17.

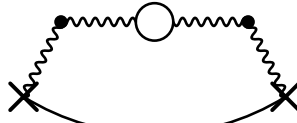


Fig. 17

Observe that all internal bosons may be renormalized to their physical masses μ , because this does not spoil non-factorizability in Fig. 17. The two factors $\mathcal{A}(q)$ in (129) are necessary in order to avoid an overcounting, but they cannot influence the presence of higher poles in Fig. 17.

Now suppose that $H(p)$ is at the $M_2 + \mu$ -threshold, $s = -p^2 = (M_2 + \mu)^2$. Then $\widetilde{D}_\mu(q-p)$ is at its μ -singularity and $\Pi(q)$ at its M_2 -singularity, and Fig. 17 corresponds (up to a normalization) to a μ - M_2 two-boson loop, i.e. Fig. 17 may effectively be substituted by Fig. 18,

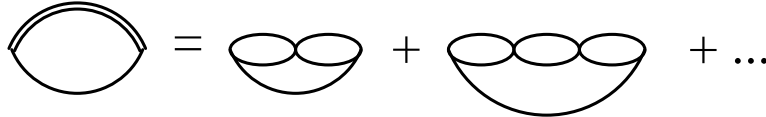


Fig. 18

where the double line represents the two-boson bound-state propagator.

Therefore, $H(p)$ is singular at $-p^2 = (M_2 + \mu)^2$, and has a large real part slightly below and a large imaginary part slightly above this threshold. As a consequence, when the contribution of $H(p)$ to $\alpha(p)$ is taken into account in the denominator $N(p)$, (118,124), it will give rise to a further μ - M_2 bound state slightly below $s = (M_2 + \mu)^2$. Further it will open the μ - M_2 decay channel at $s = (M_2 + \mu)^2$.

Now suppose we put $\Pi(q)$ in (129) on a higher (unstable) bound-state mass M_n , $n > 2$. Then in the denominator $N(q)$ of $\Pi(q)$ the real part again vanishes, but there remains an imaginary part. Therefore, $H(p)$ is finite and imaginary at $s = -p^2 = (M_n + \mu)^2$ and *cannot* give rise to a μ - M_n bound-state formation.

Further, because there is no threshold singularity at $s = (M_n + \mu)^2$, this means that *no* new decay channel opens at that point (i.e. the imaginary part of $H(p)$ varies smoothly around $s \sim (M_n + \mu^2)$), which simply means that the unstable higher n -boson bound states are no possible final states (of course, they are possible as intermediate resonances).

We could substitute the one-boson line in Fig. 17 by another $\mathcal{AG}\Pi\mathcal{A}$ line and would find that this graph behaves like a M_2 - M_2 blob near $s = (M_2 + M_2)^2$, and we could allow for even more $\mathcal{AG}\Pi\mathcal{A}$ lines. The physical picture that evolves from these considerations is like follows: in addition to the unstable n -boson bound states there exist further (unstable) bound states that are composed of Schwinger bosons μ and (stable) two-boson bound states M_2 . Further, the unstable bound states may decay into all combinations of μ and M_2 particles that are possible kinematically. The imaginary parts of the corresponding n -particle blobs (where particle means μ or M_2) are large near their thresholds, therefore there is a kinematical tendency to rise the decay probabilities for decays with *small* kinetic energy. This is not so surprising, because in $1+1$ dimensions the phase space "volume" does not grow with kinetic energy.

Further we want to emphasize the following point for later convenience. We found, by a further resummation, contributions to $N(p)$ that may be substituted by a n -particle blob that contains μ and M_2 bosons (or only M_2), *near their respective n -particle thresholds*. This is true for the *real* parts. The *imaginary* parts are given precisely by the threshold singularities which stem solely from the n -particle blobs. Therefore, the imaginary parts of these resummed contributions may be substituted by the corresponding imaginary parts of the n -particle blobs for arbitrary values of p .

Finally let us briefly comment on the special case $\theta = 0$. Here parity is conserved and we have to investigate scalar ($S\mathcal{G}\Pi(p)S$) and pseudoscalar ($P\mathcal{G}\Pi(p)P$) propagators separately. We find a partial cancellation between numerator and denominator in (117) ($\alpha(g_{\theta=0}, p) \equiv \alpha(g_{\theta=0}^*, p)$, etc.)

$$\begin{aligned} S\mathcal{G}\Pi(p)S &= \frac{m\Sigma}{1 - \alpha(g_{\theta=0}, p) - \beta(g_{\theta=0}, p)} \\ P\mathcal{G}\Pi(p)P &= \frac{m\Sigma}{1 - \alpha(g_{\theta=0}, p) + \beta(g_{\theta=0}, p)} \end{aligned} \quad (132)$$

and, therefore, using the lowest order expression (125), we find that the odd (even) n -boson blobs $d_n(p)$ are cancelled in $S\mathcal{G}\Pi(p)S$ ($P\mathcal{G}\Pi(p)P$), so that only even (odd) mass poles remain. Of course, these parity considerations may be generalized easily to the mixed bound states (where each μ is odd and each M_2 is even).

B. n -boson bound-state masses

The mass pole equation of the n -boson bound state in lowest order is given by (see (127))

$$f_n(p) := 1 - m\Sigma \cos \theta d_n(p) = 0 \quad (133)$$

For the Schwinger boson ($n = 1$) this equation reads

$$1 = m\Sigma \cos \theta \frac{-4\pi}{p^2 + \mu_0^2} \quad (134)$$

with the solution

$$-p^2 =: \mu_1^2 = \mu_0^2 + 4\pi m \Sigma \cos \theta =: \mu_0^2 + \Delta_1 \quad (135)$$

(we will denote the lowest order corrections to all the pole masses M_n^2 by Δ_n).

When we want to recover the second order result for the Schwinger mass of Section 8 we have to include all terms of $N(p)$, (118). The mass pole equation up to second order reads

$$1 = \frac{-4\pi}{p^2 + \mu_0^2} (g_1 + g_1^* + g_2 + g_2^*) + (g_1 + g_1^*) \tilde{E}_+^{(1)}(p) - g_1 g_1^* \left[(\tilde{E}_+^{(1)}(p) + \frac{-4\pi}{p^2 - \mu_0^2})^2 - (\tilde{E}_-^{(1)}(p) - \frac{-4\pi}{p^2 + \mu_0^2})^2 \right] \quad (136)$$

where g_1 (g_2) are the first (second) order contributions to g_θ (see (89)) and $\tilde{E}_\pm^{(1)}(p)$ are the exponentials $\tilde{E}_\pm(p)$ without the one-boson term, see (52). In (136), the $g_1 g_1^* (\tilde{E}_\pm^{(1)}(p))^2$ parts are, in fact, $o(m^3)$, and may be omitted. The solution to (136) is

$$\mu_2^2 := -p^2 = \mu_0^2 \left[1 + 4\pi \frac{\Sigma m}{\mu_0^2} \cos \theta + 2\pi \frac{m^2 \Sigma^2}{\mu_0^4} \left((E_+ + \tilde{E}_+^{(1)}(1)) \cos 2\theta + E_- - \tilde{E}_-^{(1)}(1) \right) \right] \quad (137)$$

and, indeed, coincides with (96) of Section 8 that was obtained by a direct perturbative calculation.

For the two-boson bound state mass in lowest order we have to solve

$$1 = \frac{1}{2!} (g_1 + g_1^*) 16\pi^2 (\widetilde{D}_\mu^2)(p) \quad (138)$$

where now μ is the *physical* Schwinger mass (137) including fermion mass corrections. $(\widetilde{D}_\mu^2)(p)$ is just the two-boson blob of Fig. 15 and may be evaluated by standard methods:

$$\begin{aligned} (\widetilde{D}_\mu^2)(p) &= \int \frac{d^2 q}{(2\pi)^2} \frac{-1}{q^2 + \mu^2} \frac{-1}{(q-p)^2 + \mu^2} = \\ &= \int \frac{d^2 q}{(2\pi)^2} \int_0^1 \frac{dx}{[q^2 + 2pq(x-1) + p^2(1-x) + \mu^2]^2} \\ &= \frac{1}{4\pi} \int_0^1 \frac{dx}{p^2 x(1-x) + \mu^2} = \frac{1}{\pi(-p^2)} \int_0^1 \frac{dy}{y^2 + (\frac{4\mu^2}{-p^2} - 1)} \\ &= \frac{1}{\pi(-p^2)} \frac{1}{R(p^2)} \arctan \frac{1}{R(p^2)}, \end{aligned} \quad (139)$$

$$R(p^2) := \sqrt{\frac{4\mu^2}{-p^2} - 1} \quad (140)$$

where we used the fact that, for the bound state, $-p^2$ has to be beyond the threshold, $-p^2 < 4\mu^2$.

Now we simply have to insert this result into (138) in order to get the mass pole:

$$1 = \frac{8\pi m \Sigma \cos \theta}{(-p^2)} \frac{1}{R(p^2)} \arctan \frac{1}{R(p^2)}. \quad (141)$$

For small fermion mass m $R(p^2)$ is very small, too. Therefore, the leading order result will stem from a matching between these two factors, where we may set $\frac{1}{-p^2} = \frac{1}{4\mu^2}$ and $\arctan \frac{1}{R(p^2)} = \frac{\pi}{2}$. Doing so we get

$$R(p^2) = \frac{\pi^2 m \Sigma \cos \theta}{\mu^2} \quad (142)$$

or

$$M_2^2 := 4\mu^2 \frac{1}{1 + \left(\frac{\pi^2 m \Sigma \cos \theta}{\mu^2}\right)^2} \simeq 4\mu^2 \left(1 - \frac{\pi^4 m^2 \Sigma^2 \cos^2 \theta}{\mu^4}\right) =: 4\mu^2 - \Delta_2, \quad (143)$$

$$M_2^2 = 4\mu^2 \left(1 - 7.83 \frac{m^2}{\mu_0^2} \cos^2 \theta + o\left(\frac{m^3}{\mu_0^3}\right)\right) \quad (144)$$

which is of second order in m . Again, this result coincides with the one from a direct perturbative calculation ([34]).

For the computation of the three-boson bound-state mass M_3 we need the three-boson propagator d_3 and find, in lowest order (see (133))

$$1 = \frac{1}{3!} m \Sigma \cos \theta \cdot 64\pi^3 \widetilde{D}_\mu^3(p) \quad (145)$$

or, after a rescaling $p \rightarrow \frac{p}{\mu}$ to dimensionless momenta

$$1 = \frac{64\pi^3}{6} \frac{m \Sigma}{\mu^2} \cos \theta \widetilde{D}_\mu^3(p). \quad (146)$$

$\widetilde{D}_\mu^3(p)$ is given by the three-boson loop of Fig. 15 (in the sequel we introduce positive squared momentum $s = -p^2 > 0$)

$$\begin{aligned} \widetilde{D}_\mu^3(p) &= - \int \frac{d^2 q_1 d^2 q_2}{(2\pi)^4} \frac{1}{(p + q_1 + q_2)^2 + 1} \frac{1}{q_1^2 + 1} \frac{1}{q_2^2 + 1} = \\ &-2 \int_0^1 dx \int_0^x dy \int \frac{d^2 q_1 d^2 q_2}{(2\pi)^4} \frac{1}{\left[q_1^2 + 1 + (q_2^2 - q_1^2)x + ((p + q_1 + q_2)^2 - q_2^2)y\right]^3} = \\ &\int \frac{dx}{(4\pi)^2} \int_0^x \frac{dy}{s(xy - x^2y - y^2 + xy^2) - x + x^2 - xy + y^2} = \\ &\int \frac{dx}{8\pi^2(1 - s(1 - x))} \int_0^{\frac{x}{2}} \frac{dz}{z^2 + T^2(s, x)} = \end{aligned}$$

$$\int_0^1 \frac{dx}{8\pi^2(1-s(1-x))} \frac{1}{T(s,x)} \arctan \frac{x}{2T(s,x)}, \quad (147)$$

$$T^2(s,x) = \frac{x^2 - sx^2(1-x) + 4x(1-x)}{4(s(1-x) - 1)}, \quad (148)$$

where, as usual, we introduced Feynman parameter integrals and performed the momentum integrations. Further, the first Feynman parameter integral could be done analytically. The numerator of T^2 has a double zero at $s = 9$:

$$9x(x - \frac{2}{3})^2. \quad (149)$$

This double zero is in the integration range of x and is precisely the threshold singularity. Setting

$$s = 9 - \Delta_3 \quad (150)$$

in the numerator of T^2 in the factor $\frac{1}{T}$, and $s = 9$ everywhere else, where it is safe, one arrives at:

$$\frac{1}{12\pi^2} \int_0^1 \frac{dx}{\sqrt{|9x-8|}} \frac{\arctan \frac{\sqrt{x|9x-8|}}{3(x-\frac{2}{3})}}{\sqrt{(x-\frac{2}{3})^2x + \frac{\Delta_3}{9}x^2(1-x)}} =: I(\Delta_3). \quad (151)$$

The mass-pole equation reads

$$1 = \frac{64\pi^3}{6} m\Sigma \cos \theta I(\Delta_3) \quad (152)$$

and must be evaluated numerically. It gives rise to an extremely tiny mass correction Δ_3 . For sufficiently small m it is very well saturated by

$$\Delta_3(m\Sigma \cos \theta) \simeq 6.993 \exp(-\frac{0.263}{m\Sigma \cos \theta}) \quad (153)$$

and is therefore smaller than polynomial in m . (I checked the numerical formula (153) for $30 < \frac{1}{m\Sigma \cos \theta} < 1000$, corresponding to $10^{-2} < \Delta_3 < 10^{-100}$, but I am convinced that it remains true for even larger $\frac{1}{m\Sigma \cos \theta}$; however, there the numerical integration is quite difficult because of the pole in (151).)

We conclude that the three-boson bound state mass is nearly entirely given by three times the Schwinger boson mass (we change back to dimensionfull quantities now),

$$M_3^2 = 9\mu^2 - \Delta_3 \quad , \quad \Delta_3 = 6.993\mu^2 \exp(-0.263 \frac{\mu^2}{m\Sigma \cos \theta}) \quad (154)$$

or, differently stated, that the binding of three bosons is extremely weak.

Therefore it holds that $M_3 > \mu + M_2$, and, consequently, a decay of M_3 into $\mu + M_2$ is possible. This has the consequence that the three-boson bound state is unstable even for $\theta = 0$.

C. A mixed bound-state mass

For our further discussion we will need the residues of the propagator $\Pi(p)$ at its various mass poles. The n -boson mass poles were, in leading order, the zeros of the functions $f_n(p)$, see (153). Therefore, we need the first Taylor coefficient c_n of each $f_n(p)$ at its mass pole $M_n^2 = (n\mu)^2 - \Delta_n$ ($n \geq 2$) or $M_1^2 = \mu_0^2 + \Delta_1$,

$$f_n(s) \simeq c_n(s - M_n^2) \quad , \quad c_n = \frac{d}{ds} f_n(s)|_{s=M_n^2} \quad (155)$$

where $s = -p^2$. The c_n may be easily obtained from our mass computations. From (134) and (141) we find for c_1 and c_2

$$c_1 = \frac{1}{4\pi m \Sigma \cos \theta} = \frac{1}{\Delta_1} \quad (156)$$

$$c_2 = \frac{\mu^2}{8\pi^4 (m \Sigma \cos \theta)^2} = \frac{1}{2\Delta_2} \quad (157)$$

For the computation of c_3 we observe that because of formulae (150), (153) $m \Sigma \cos \theta d_3(s)$ may be written, in the vicinity of $s = M_3^2$, like

$$m \Sigma \cos \theta d_3(s) \sim \frac{m \Sigma \cos \theta}{0.263} \ln \frac{6.993\mu^2}{9\mu^2 - s}. \quad (158)$$

Therefore, we find the Taylor coefficient

$$c_3 = \frac{m \Sigma \cos \theta}{0.263 \Delta_3}. \quad (159)$$

Further we need, for the computation of the lowest mixed bound-state mass $M_{1,1}$ (which is composed of one M_2 and one $\mu \equiv M_1$), the residues of the propagator $\Pi(p)$ at the two lowest mass poles. The denominator $N(p)$, (118), is given by (155), and for the numerator of $\Pi(p)$, (117), we use $\alpha(g_\theta, s \sim M_n^2) \sim g_\theta \bar{E}_+(s \sim M_n^2) \sim \frac{g_\theta}{g_\theta + g_\theta^*}$, etc., which holds near the pole, see (124) – (127), and find (here $n = 1, 2$)

$$\Pi(s \sim M_n^2) \sim \frac{1}{(g_\theta + g_\theta^*)c_n(s - M_n^2)} \begin{pmatrix} g_\theta & (-1)^n g_\theta^* \\ (-1)^n g_\theta & g_\theta^* \end{pmatrix} \quad (160)$$

For the computation of the μ - M_2 bound state we need, in addition, the matrix \mathcal{A} , (113), at the n -boson mass poles (here $n \neq 1$, because there \mathcal{A} itself has a pole like (160)),

$$\mathcal{A}(s = M_n^2) = \frac{1}{g_\theta + g_\theta^*} \begin{pmatrix} 1 & (-1)^n \\ (-1)^n & 1 \end{pmatrix} \quad (161)$$

Now we are prepared for the computation of the $M_{1,1}$ mixed bound-state mass. In Subsection 10.1 we claimed that we could substitute the resummed contribution $H(p)$ to $N(p)$, see (129) and Fig. 17, near its threshold by a two-particle blob consisting of one μ and one M_2 (times a

not yet specified factor), see Fig. 18. This we achieve by inserting expression (160) for $\Pi(p)$ near its two poles μ , M_2 , into (129), and by using (161) for the remaining $\mathcal{A}(-q^2 \sim M_2^2)$. Altogether we find for $H(p)$ near its threshold

$$\begin{aligned}
H_{ii'}(-p^2 \sim (M_2 + \mu)^2) &\sim \int \frac{d^2 q}{(2\pi)^2} \delta_{ijk} \frac{1}{g_\theta + g_\theta^*} \begin{pmatrix} 1 & 1 \\ 1 & 1 \end{pmatrix}_{jj'} \begin{pmatrix} g_\theta & 0 \\ 0 & g_\theta^* \end{pmatrix}_{j'l} \frac{1}{(g_\theta + g_\theta^*)c_2(-q^2 - M_2^2)} \\
&\cdot \begin{pmatrix} g_\theta & g_\theta^* \\ g_\theta & g_\theta^* \end{pmatrix}_{ll'} \frac{1}{g_\theta + g_\theta^*} \begin{pmatrix} 1 & 1 \\ 1 & 1 \end{pmatrix}_{l'k'} \frac{1}{(g_\theta + g_\theta^*)c_1(-(q-p)^2 - \mu^2)} \begin{pmatrix} 1 & -1 \\ -1 & 1 \end{pmatrix}_{km} \delta_{i'k'm} = \\
&\delta_{ijk} \begin{pmatrix} 1 & 1 \\ 1 & 1 \end{pmatrix}_{jj'} \begin{pmatrix} 1 & -1 \\ -1 & 1 \end{pmatrix}_{kk'} \delta_{i'j'k'} \int \frac{d^2 q}{(2\pi)^2} \frac{1}{(g_\theta + g_\theta^*)^2 c_1 c_2 (-q^2 - M_2^2) (-(q-p)^2 - \mu^2)} \quad (162)
\end{aligned}$$

The contribution of $H_{ii'}$ to $\alpha(g_\theta) + \alpha(g_\theta^*)$ in the denominator $N(p)$, (124), is

$$\begin{aligned}
g_\theta H_{++}(p) + g_\theta^* H_{--}(p) &=: (g_\theta + g_\theta^*) d_{1,1}(p) = \\
(g_\theta + g_\theta^*) \int \frac{d^2 q}{(2\pi)^2} \frac{8\pi^4 m \Sigma \cos \theta}{\mu^2 (q^2 + M_2^2)} \frac{4\pi}{(p-q)^2 + \mu^2} = \\
\frac{32\pi^5 m^2 \Sigma^2 \cos^2 \theta}{2\pi \mu^2 \bar{w}(s, M_2^2, \mu^2)} \left(\pi + \right. \\
\left. \arctan \frac{2s}{\bar{w}(s, M_2^2, \mu^2) - \frac{1}{\bar{w}(s, M_2^2, \mu^2)} (s + \mu^2 - M_2^2)(s - \mu^2 + M_2^2)} \right) \quad (163)
\end{aligned}$$

$$\bar{w}(x, y, z) := (-x^2 - y^2 - z^2 + 2xy + 2xz + 2yz)^{\frac{1}{2}} \quad (164)$$

where $s = -p^2 \sim (\mu + M_2)^2$. The μ - M_2 bound-state mass fulfills the equation

$$1 = (g_\theta + g_\theta^*) d_{1,1}(p) \quad (165)$$

with the solution in leading order (here $M_{1,1}$ denotes the μ - M_2 bound-state mass)

$$M_{1,1}^2 = (\mu + M_2)^2 - \Delta_{1,1} \quad , \quad \Delta_{1,1} = \frac{32\pi^{10} (m \Sigma \cos \theta)^4}{\mu^6} \quad (166)$$

which is valid for sufficiently small $\Delta_{1,1}$. $M_{1,1}$ was computed from a two-boson blob (Fig. 18), like M_2 , therefore the Taylor coefficient of $(s - M_{1,1}^2)$ is analogous to c_2 , equ. (157),

$$c_{1,1} = \frac{1}{2\Delta_{1,1}} = \frac{\mu^6}{64\pi^{10} (m \Sigma \cos \theta)^4}. \quad (167)$$

Further, the above equ. (162) shows that the μ - M_2 blob $d_{1,1}(p)$ enters into the functions α , β of \mathcal{A} , (113), like any other odd n -boson blob $d_n(p)$.

In principle, even higher mixed bound-state masses could be computed along similar lines, but we want to change now to the computation of the decay widths of the lowest unstable bound states.

D. Decay width computations

In order to find the decay widths of some bound states, we have to examine the imaginary parts of the denominator $N(p)$ in the vicinity of the corresponding mass poles. Using the first order approximation (125) for α, β we find for $N(p)$ (e.g. in the vicinity of $s \sim M_3^2$ for definiteness)

$$\begin{aligned} N(p) &\simeq 1 - m\Sigma \cos \theta \tilde{E}_+(p) + \frac{m^2 \Sigma^2}{4} (\tilde{E}_+^2(p) - \tilde{E}_-^2(p)) \\ &= 1 - m\Sigma \cos \theta (d_1(p) + d_2(p) + d_{1,1}(p) + d_3(p) + \dots) + \\ &\quad m^2 \Sigma^2 (d_1(p)(d_2(p) + d_4(p) + \dots) + d_{1,1}(p)(d_2(p) + d_4(p) + \dots) + \\ &\quad d_3(p)(d_2(p) + d_4(p) + \dots) + \dots) \end{aligned} \quad (168)$$

where we included the μ - M_2 blob $d_{1,1}$, as discussed above, because we need it for the subsequent discussion (we ignore, for the moment, higher M_2 blobs that are, in principle, present). Near $s = M_3^2$ the real part of (168) is given by $c_3(s - M_3^2)$ and we find

$$\begin{aligned} N(s \sim M_3^2) &\sim c_3(s - M_3^2) - im\Sigma \cos \theta (\text{Im} d_2(s \sim M_3^2) + \text{Im} d_{1,1}(s \sim M_3^2)) + \\ &\quad im^2 \Sigma^2 d_3(s \sim M_3^2) \text{Im} d_2(s \sim M_3^2) + o(m^2) \\ &= c_3(s - M_3^2) - im\Sigma (\cos \theta - \frac{1}{\cos \theta}) \text{Im} d_2(M_3^2) - im\Sigma \cos \theta \text{Im} d_{1,1}(M_3^2) + o(m^2) \end{aligned} \quad (169)$$

where we used $d_3(M_3^2) \sim \frac{1}{m\Sigma \cos \theta}$, see (133).

This computation may be generalized and tells us that parity forbidden imaginary parts (decay channels) acquire a factor $(\cos \theta - \frac{1}{\cos \theta})$, whereas parity allowed imaginary parts have the usual $\cos \theta$ factor.

[*Remark:* There seems to be something wrong with the sign of the parity forbidden imaginary part (the d_2 term). Actually the sign is o.k. and the problem is a remnant of the Euclidean conventions that are implicit in the whole computation (see Section 1). In these conventions θ is imaginary and therefore $(\cos \theta - \frac{1}{\cos \theta}) \geq 0$. Of course, this is not a reasonable convention for a final result. When performing the whole computation in Minkowski space and for real θ , roughly speaking, the roles of E_+ and E_- are exchanged in (168). This gives an additional relative sign between parity even and odd n -boson propagators and, therefore, changes the factor of d_2 to $(\frac{1}{\cos \theta} - \cos \theta)$, which is ≥ 0 for real θ . We will keep this remark in mind and express the final results in Minkowski space and for real θ .]

Now we may find the M_3 decay widths by comparing the inverse of (169) to the general formula

$$G(p) \sim \frac{\text{const.}}{s - M^2 - iM\Gamma}, \quad (170)$$

where Γ is the decay width. We find (for real θ)

$$\frac{1}{N(s \sim M_3^2)} \simeq \frac{\text{const.}}{s - M_3^2 - i \frac{m\Sigma}{c_3} \left[(\frac{1}{\cos \theta} - \cos \theta) \text{Im} d_2(M_3^2) + \cos \theta \text{Im} d_{1,1}(M_3^2) \right]}. \quad (171)$$

Next we need the imaginary parts $\text{Im } d_2$, $\text{Im } d_{1,1}$. Both of them stem from a two-boson blob, so let us write down the general result (which is standard) ($s = -p^2$)

$$\begin{aligned} \text{Im}(D_{M_1}\widetilde{D_{M_2}})(s) &= \text{Im} \int \frac{d^2q}{(2\pi)^2} \frac{-1}{q^2 + M_1^2} \frac{-1}{(p-q)^2 + M_2^2} \\ &= \frac{1}{2w(s, M_1^2, M_2^2)}, \end{aligned} \quad (172)$$

$$w(x, y, z) = (x^2 + y^2 + z^2 - 2xy - 2xz - 2yz)^{\frac{1}{2}}. \quad (173)$$

Therefore we can write for (171) (where the normalization factors of d_2 and $d_{1,1}$ are $\frac{c_2^2}{2}$ and c_1c_2 , respectively)

$$\frac{\text{const.}}{s - M_3^2 - i\frac{m\Sigma}{c_3}(\frac{1}{\cos\theta} - \cos\theta)\frac{4\pi^2}{w(M_3^2, \mu^2, \mu^2)} - i\frac{(m\Sigma \cos\theta)^2}{c_3}\frac{16\pi^5}{\mu^2 w(M_3^2, \mu^2, M_2^2)}} \quad (174)$$

and therefore, by using the approximations

$$w(M_3^2, \mu^2, \mu^2) \simeq w(9\mu^2, \mu^2, \mu^2) = 3\sqrt{5}\mu^2 \quad (175)$$

$$w(M_3^2, M_2^2, \mu^2) \simeq w(9\mu^2, M_2^2, \mu^2) = 2\sqrt{3}\mu\sqrt{\Delta_3} + o(m^2), \quad (176)$$

we find the following results:

$$\begin{aligned} \Gamma_{M_3 \rightarrow 2\mu} &= 0.263 \frac{4\pi^2 \Delta_3}{9\sqrt{5}\mu} \left(\frac{1}{\cos^2\theta} - 1 \right) \\ &\simeq 3.608\mu \left(\frac{1}{\cos^2\theta} - 1 \right) \exp(-0.929 \frac{\mu}{m \cos\theta}) \end{aligned} \quad (177)$$

and

$$\begin{aligned} \Gamma_{M_3 \rightarrow \mu + M_2} &= 0.263 \frac{4\pi^3 \Delta_3}{3\sqrt{3}\mu} \\ &\simeq 43.9\mu \exp(-0.929 \frac{\mu}{m \cos\theta}) \end{aligned} \quad (178)$$

where we inserted the numerical value $\Sigma = \frac{e\gamma\mu}{2\pi} = 0.283\mu$.

The ratio of the two partial decay widths does not depend on the approximations that were used for the M_3 computation,

$$\frac{\Gamma_{M_3 \rightarrow 2\mu}}{\Gamma_{M_3 \rightarrow \mu + M_2}} = \frac{\frac{1}{\cos^2\theta} - 1}{\sqrt{15}\pi}. \quad (179)$$

Analogously we may compute the decay width of the mixed bound state $M_{1,1}$, starting from

$$N(s \sim M_{1,1}^2) \simeq c_{1,1}(s - M_{1,1}^2) - im\Sigma(\frac{1}{\cos\theta} - \cos\theta)\text{Im}d_2(M_{1,1}^2) \quad (180)$$

which leads to the decay width

$$\Gamma_{M_{1,1} \rightarrow 2\mu} = \frac{2^8 \pi^{12} (m \Sigma \cos \theta)^5}{9 \sqrt{5} \mu^9} \left(\frac{1}{\cos^2 \theta} - 1 \right) \simeq 21340 \mu \left(\frac{m \cos \theta}{\mu} \right)^5 \left(\frac{1}{\cos^2 \theta} - 1 \right) \quad (181)$$

for the decay $M_{1,1} \rightarrow 2\mu$. This decay is parity forbidden, and therefore $M_{1,1}$ is stable for $\theta = 0$.

In principle, we could have computed the above decay widths by another method, too, namely by the use of the resummed three-point function of Fig. 12. Choosing the first graph on the r.h.s. of Fig. 12 (consisting of three exact propagators and one pure vertex), we could precisely rederive our results (177), (178), and (181).

XI. SCATTERING

A. Two-dimensional kinematics

For a discussion of scattering processes we need some basic facts about two-dimensional kinematics. We will restrict our discussion to elastic scattering. Suppose we have two incoming particles with masses M_1 , M_2 and momenta p_1 , p_2 , and two outgoing particles, again with masses M_1 , M_2 , and with momenta p_3 , p_4 . Momentum conservation requires

$$p := p_1 + p_2 = p_3 + p_4 \quad (182)$$

and all momenta are *Minkowskian* in the sequel. In the center of mass system we may write

$$\begin{aligned} p_1 &= \begin{pmatrix} \sqrt{k^2 + M_1^2} \\ k \end{pmatrix}, & p_2 &= \begin{pmatrix} \sqrt{k^2 + M_2^2} \\ -k \end{pmatrix} \\ p_3 &= \begin{pmatrix} \sqrt{k^2 + M_1^2} \\ \pm k \end{pmatrix}, & p_4 &= \begin{pmatrix} \sqrt{k^2 + M_2^2} \\ \mp k \end{pmatrix} \end{aligned} \quad (183)$$

where in p_3 , p_4 the first sign is for transmission, the second sign is for reflexion. For the kinematical variables we find for transmission

$$\begin{aligned} s &= (p_1 + p_2)^2 = 2k^2 + M_1^2 + M_2^2 + 2\sqrt{(k^2 + M_1^2)(k^2 + M_2^2)} \\ t_T &= (p_1 - p_4)^2 = -2k^2 + M_1^2 + M_2^2 - 2\sqrt{(k^2 + M_1^2)(k^2 + M_2^2)} \\ u_T &= (p_1 - p_3)^2 = 0 \end{aligned} \quad (184)$$

and for reflexion

$$\begin{aligned} s &= (p_1 + p_2)^2 = 2k^2 + M_1^2 + M_2^2 + 2\sqrt{(k^2 + M_1^2)(k^2 + M_2^2)} \\ t_R &= (p_1 - p_4)^2 = 2k^2 + M_1^2 + M_2^2 - 2\sqrt{(k^2 + M_1^2)(k^2 + M_2^2)} \\ u_R &= (p_1 - p_3)^2 = -4k^2 \end{aligned} \quad (185)$$

When the two masses are equal, the two particles are identical in our theory and the discrimination between transmission and reflexion does not make sense. The kinematical variables turn into

$$\begin{aligned}s &= (p_1 + p_2)^2 = 4(k^2 + M^2) \\ t &= (p_1 - p_4)^2 = -4k^2 \\ u &= (p_1 - p_3)^2 = 0\end{aligned}\tag{186}$$

The elastic scattering cross section of two particles is given by

$$\sigma_{M_a M_b \rightarrow M_a M_b}(s) = \frac{C_{\text{sym}} |\mathcal{M}(s)|^2}{2w^2(s, M_a^2, M_b^2)}\tag{187}$$

where w is defined in (173), \mathcal{M} is the transition matrix element and C_{sym} is a symmetry factor that takes into account identical particles in the final state ($C_{\text{sym}} = \frac{1}{n_1!n_2!}$ for n_1 particles M_1 and n_2 particles M_2 in the final state). As it stands, expression (187) holds provided that the initial and final particle propagators are normalized in the usual fashion ($\sim \frac{1}{s-M_i^2}$). Otherwise, (187) is multiplied by the normalization factors (the residues of the propagators).

B. Scattering processes

Finally we are prepared for a discussion of scattering. Let us focus for the moment on the lowest order graph of Fig. 14 for the four-point function (123). It consists of four external exact propagators $\Pi(p_i)$ and a simple vertex as the lowest order transition matrix element. The $\Pi(p_i)$ contain two stable-particle mass poles, μ and M_2 , therefore this graph describes μ and M_2 scattering (this remains true for higher order contributions; as a consequence, the same transition matrix elements contribute to μ and M_2 scattering processes, and they may only differ by some kinematical and normalization factors).

Let us consider elastic scattering of two Schwinger bosons for definiteness. Then each external $\Pi(p_i)$ propagator is odd and contributes to the graph like ($s_i = -p_i^2$)

$$\Pi_{jk}(s_i = \mu^2)P_k = \frac{4\pi(g_\theta + g_\theta^*)}{s_i - \mu^2} \begin{pmatrix} 1 \\ -1 \end{pmatrix}_j\tag{188}$$

Here we face the problem that the first graph of Fig. 14 is already of fifth order, because each propagator $\Pi(s_i)$ has an external vertex. We just omit these external vertices (i.e. we omit the factor $(g_\theta + g_\theta^*)$ in (188) for each propagator), because we want to discuss first order scattering. Doing so, we find for this graph

$$P_{j_1}P_{j_2}P_{j_3}P_{j_4}\delta_{j_1j_2k_1}\mathcal{G}_{k_1k_2}\delta_{j_3j_4k_2}\prod_{i=1}^4\frac{4\pi}{s_i - \mu^2} = (g_\theta + g_\theta^*)\prod_{i=1}^4\frac{4\pi}{s_i - \mu^2}\tag{189}$$

i.e. each μ propagator has a residue 4π . In order to obtain the transition matrix element one has to amputate the external boson propagators in the usual LSZ fashion. When the propagators are normalized by $r_1 = 4\pi$, the bosons themselves are normalized by $\sqrt{4\pi}$, which

has to be divided out for each amputation. This leaves a factor $\sqrt{4\pi}$ for each external boson in the transition matrix element. However, the squared transition matrix element enters the scattering cross section, therefore the net effect on the cross section is a multiplication by the corresponding propagator residue r_i for each external line.

Therefore, we find for the lowest order boson-boson elastic scattering

$$\sigma_{\mu+\mu\rightarrow\mu+\mu}(s) = r_1^4 \frac{\frac{1}{2}(m\Sigma \cos \theta)^2}{2w^2(s, \mu^2, \mu^2)} \quad (190)$$

where we have for the propagator residues (they may be inferred from (160), $r_i = \frac{1}{c_i(g_\theta + g_\theta^*)}$)

$$r_1 = 4\pi \quad , \quad r_2 = \frac{8\pi^4 m \Sigma \cos \theta}{\mu^2}. \quad (191)$$

(190), of course, coincides with a naive computation using the first order bosonic four-point function $\langle \Phi(x_1) \dots \Phi(x_4) \rangle_m^c$ (the latter may be inferred immediately from (48)). Observe that (190) is singular at the real particle production threshold $s = 4\mu^2$ ($w(4\mu^2, \mu^2, \mu^2) = 0$).

In a next step we want to consider the second order contribution of Fig. 14 (the third type graphs). There are three graphs of this type, namely s , t and u channel, but we will consider only the s channel (annihilation channel) for the moment. In this diagram the lowest order graph must be subtracted in order to avoid overcounting (see Fig. 14), therefore the graph of Fig. 19

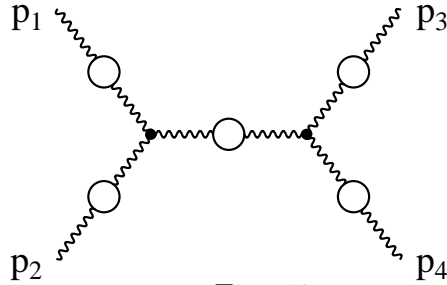


Fig. 19

contains the lowest order graph and the second order s channel contribution.

Actually we will allow for arbitrary final states in the sequel, $\mu + \mu \rightarrow f$, because this enables us to use the optical theorem, which may be written for the current problem like

$$\sigma_{ab \rightarrow f}^{\text{tot}}(s) = \frac{r_a r_b}{w(s, M_a^2, M_b^2)} \text{Im} \mathcal{M}_{ab \rightarrow ab}(s) \quad (192)$$

where $\mathcal{M}_{ab \rightarrow ab}$ is the forward elastic scattering amplitude. $w(s, M_a^2, M_b^2)$ is an initial state velocity factor; the final state factors must be produced by $\mathcal{M}_{ab \rightarrow ab}$, as we will find in the sequel.

Specifically we choose $a = b = \mu$, and, therefore, both vertices of \mathcal{M} are contracted by scalars S (we use matrix notation)

$$\mathcal{M}_{2\mu \rightarrow 2\mu}(s) = S^T \mathcal{G} \Pi(s) S \quad (193)$$

Before starting the computations, we want to make some comments. First, as is obvious from Fig. 19 and our discussion, in (192) all combinations of $n_1 \mu$ and $n_2 M_2$ are allowed as

final states. Consequently, they must exist as intermediate states in $\mathcal{M}_{2\mu \rightarrow 2\mu}$, too, in order to saturate the optical theorem (192). Therefore, we are forced to include the M_2 particle into the two-point function $\Pi(p)$, as we did in the previous section, in order to maintain unitarity.

Secondly, in finite order perturbation theory the optical theorem relates graphs of different order. However, we use a resummed perturbation series in (192) and, therefore, we will find a relation that holds for the whole, resummed two-point function $\Pi(s)$.

In a first step we want to discuss the special case $\theta = 0$, because it is much easier and shows the relevant features without technical complications. For $\theta = 0$ the amplitude (193) reads (see (132))

$$\begin{aligned}\mathcal{M}_{2\mu \rightarrow 2\mu}^{\theta=0}(s) &= \frac{m\Sigma}{1 - \frac{m\Sigma}{2}(\tilde{E}_+(s) + \tilde{E}_-(s))} \\ &= \frac{m\Sigma}{1 - m\Sigma(d_2(s) + d_{2,0}(s) + d_4(s) + \dots)}\end{aligned}\quad (194)$$

where we inserted the lowest order (125) and expanded the exponentials $\tilde{E}_{\pm}(s)$ like in (126). Again, we include the M_2 particle (which is found by a further resummation) into \tilde{E}_{\pm} , because this is absolutely necessary, as we have just argued. Actually $d_{2,0}$ describes the M_2 - M_2 blob, and in (194) only parity even contributions may occur. For the optical theorem (192) we need the imaginary part

$$\text{Im}\mathcal{M}_{2\mu \rightarrow 2\mu}^{\theta=0}(s) = \frac{m^2\Sigma^2(\text{Im}d_2(s) + \text{Im}d_{2,0}(s) + \text{Im}d_4(s) + \dots)}{[1 - m\Sigma(\text{Re}d_2(s) + \dots)]^2 + m^2\Sigma^2(\text{Im}d_2(s) + \dots)^2}\quad (195)$$

We find the following physical picture: at $s = 4\mu^2$ the elastic scattering threshold ($f = 2\mu$) opens, at $s = 4M_2^2$ the $2\mu \rightarrow 2M_2$ threshold is added, at $s = 16\mu^2$ the $2\mu \rightarrow 4\mu$ threshold, etc. The $d_n(s)$ were defined as $d_n(s) = \frac{r_1^n}{n!}\widetilde{D}_\mu^n(s)$, therefore their imaginary parts are precisely the final state factors for the corresponding cross section, including the phase space integration (the cutting of the $\widetilde{D}_\mu^n(s)$), the propagator normalizations $r_1 = 4\pi$, and the final state symmetry factors for n identical particles, $C_{\text{sym}} = \frac{1}{n!}$. For the multi- M_2 propagators $d_{m,0}(s)$ (and, more generally, for $d_{m,n}(s)$) the first two points (propagators with their residues) are obvious, the third one (correct $\frac{1}{m!}$ final state symmetry factor) may be checked by a closer inspection of the mass perturbation series. We show it for the lowest order contribution to the M_2 - M_2 propagator $d_{2,0}(s)$, where we depict in Fig. 20 this lowest order contribution and the perturbation expansion graph where it stems from.



Fig. 20

The second graph in Fig. 20 is a second order mass perturbation, therefore it contains a factor $\frac{m^2}{2!}$. Further there exists precisely one diagram of this kind in the perturbation series, therefore the $\frac{1}{2!}$ factor remains in $d_{2,0}(s)$ as the required final space symmetry factor. Via some combinatorics this argument may be generalized to higher order contributions to the M_2 - M_2 loop $d_{2,0}(s)$ and to higher multi- M_2 loops.

For the total cross section (192) we get

$$\sigma_{2\mu \rightarrow f}^{\text{tot}, \theta=0}(s) = \frac{r_1^2 m^2 \Sigma^2 (\text{Im}d_2(s) + \text{Im}d_{2,0}(s) + \text{Im}d_4(s) + \dots)}{w(s, \mu^2, \mu^2) ([1 - m\Sigma(\text{Re}d_2(s) + \dots)]^2 + m^2 \Sigma^2 (\text{Im}d_2(s) + \dots)^2)} \quad (196)$$

$$\text{Im}d_2(s) = \frac{r_1^2}{2!} \frac{1}{2w(s, \mu^2, \mu^2)} \quad \text{etc.} \quad (197)$$

which we want to evaluate for some specific values of s . At the elastic scattering threshold $s = 4\mu^2$, $\text{Im}d_2(s)$ is singular and we find

$$\sigma_{2\mu \rightarrow f}^{\text{tot}, \theta=0}(4\mu^2) = 4. \quad (198)$$

Therefore, the singular behaviour of the lowest order cross section at $s = 4\mu^2$ is cancelled by higher order contributions. This behaviour is, however, further changed by the t and u channel contributions.

In an intermediate range, far from all thresholds and bound state masses, $4\mu^2 < s < 4M_2^2$, σ^{tot} is well described by the lowest order result (190), because there $m\Sigma d_n(s)$ is small compared to 1,

$$\sigma_{2\mu \rightarrow f}^{\text{tot}, \theta=0}(s) \simeq \frac{r_1^2 m^2 \Sigma^2 \text{Im}d_2(s)}{w(s, \mu^2, \mu^2)} = \frac{\frac{1}{2!} r_1^4 m^2 \Sigma^2}{2w^2(s, \mu^2, \mu^2)}. \quad (199)$$

At the first bound-state mass, $s = M_{2,0}^2 < 4M_2^2$, a resonance occurs. There the real part contribution to the denominator of (196) vanishes by definition and we find

$$\sigma_{2\mu \rightarrow f}^{\text{tot}, \theta=0}(M_{2,0}^2) = \frac{r_1^2 m^2 \Sigma^2 \text{Im}d_2(M_{2,0}^2)}{w(M_{2,0}^2, \mu^2, \mu^2) m^2 \Sigma^2 (\text{Im}d_2(M_{2,0}^2))^2} = 4 \quad (200)$$

and the resonance height does not depend on the coupling constant (of course, the width does).

At the $2M_2$ production threshold $s = 4M_2^2$ the scattering cross section goes down to zero (here $d_{2,0}$ is singular)

$$\sigma_{2\mu \rightarrow f}^{\text{tot}, \theta=0}(4M_2^2) \simeq \frac{r_1^2 m^2 \Sigma^2}{w(4M_2^2, \mu^2, \mu^2)} \frac{\text{Im}d_{2,0}(4M_2^2)}{m^2 \Sigma^2 (\text{Im}d_{2,0}(4M_2^2))^2} = 0. \quad (201)$$

In addition, at this point the $2\mu \rightarrow 2M_2$ production channel opens. At the four-boson bound-state mass $s = M_4^2$ we find the next resonance

$$\sigma_{2\mu \rightarrow f}^{\text{tot}, \theta=0}(M_4^2) = \frac{r_1^2 (\text{Im}d_2(M_4^2) + \text{Im}d_{2,0}(M_4^2))}{w(M_4^2, \mu^2, \mu^2) (\text{Im}d_2(M_4^2) + \text{Im}d_{2,0}(M_4^2))^2} \quad (202)$$

Again, the resonance height does not depend on the coupling constant, and, in addition, here already two decay channels are open for the M_4 resonance.

At the $2\mu \rightarrow 4\mu$ real production threshold $s = 16\mu^2$, σ^{tot} again vanishes, and for even higher s the above pattern repeats.

Observe that, because σ^{tot} has a local maximum (resonance) at the bound-state masses, whereas it is zero at the real particle production thresholds, the resonance widths (decay widths) *must* be bounded by the binding energies. For the $M_{1,1}$ and M_3 decay widths this may be seen from the explicit results (177), (178) and (181).

The t and u channel contributions do not change this pattern (they have no imaginary parts and are small for all t, u).

Next let us turn to the $\theta \neq 0$ case. There parity forbidden transitions are possible, and therefore we will find $M_{1,1}$ and M_3 resonances, too. The forward scattering amplitude (193) reads

$$\mathcal{M}_{2\mu \rightarrow 2\mu}(s) = \frac{g_\theta + g_\theta^* - 2g_\theta g_\theta^*(\tilde{E}_+(s) - \tilde{E}_-(s))}{1 - (g_\theta + g_\theta^*)\tilde{E}_+(s) + g_\theta g_\theta^*(\tilde{E}_+^2(s) + \tilde{E}_-^2(s))} =$$

$$\frac{g_\theta + g_\theta^* - 4g_\theta g_\theta^*(d_1(s) + d_{1,1}(s) + d_3(s) + \dots)}{1 - (g_\theta + g_\theta^*)(d_1(s) + d_2(s) + d_{1,1}(s) + \dots) + 4g_\theta g_\theta^*[d_1(s)(d_2(s) + d_{2,0}(s) + \dots) + \dots]} \quad (203)$$

Please observe the presence of only odd d_i in the numerator and of only odd \times even $d_i \times d_j$ in the second term of the denominator. Therefore, the $4g_\theta g_\theta^*$ terms in the numerator and denominator do not contribute to parity allowed transitions, and the discussion of such parity allowed transitions is analogous to the $\theta = 0$ case that we discussed above.

Again, we want to discuss the scattering cross section

$$\sigma_{2\mu \rightarrow f}^{\text{tot}}(s) = \frac{r_1^2}{w(s, \mu^2, \mu^2)} \text{Im} \mathcal{M}_{2\mu \rightarrow 2\mu}(s) \quad (204)$$

for some specific values of s . At $s = 4\mu^2$ we find again

$$\sigma_{2\mu \rightarrow f}^{\text{tot}}(4\mu^2) = \frac{r_1^2}{w(4\mu^2, \mu^2, \mu^2)} \frac{(g_\theta + g_\theta^*)^2 \text{Im} d_2(4\mu^2)}{1 + (g_\theta + g_\theta^*)^2 (\text{Im} d_2(4\mu^2))^2} = 4 \quad (205)$$

At the first parity forbidden resonance $s = M_{1,1}^2$ we find ($\text{Red}_{1,1} = \frac{1}{g_\theta + g_\theta^*}$)

$$\sigma_{2\mu \rightarrow f}^{\text{tot}}(M_{1,1}^2) \simeq \frac{r_1^2}{w(M_{1,1}^2, \mu^2, \mu^2)} \text{Im} \frac{g_\theta + g_\theta^* - 4g_\theta g_\theta^* \text{Red}_{1,1}(M_{1,1}^2)}{-i(g_\theta + g_\theta^*) \text{Im} d_2(M_{1,1}^2) + 4ig_\theta g_\theta^* \text{Red}_{1,1}(M_{1,1}^2) \text{Im} d_2(M_{1,1}^2)}$$

$$= \frac{r_1^2}{w(M_{1,1}^2, \mu^2, \mu^2)} \frac{\left(g_\theta + g_\theta^* - \frac{4g_\theta g_\theta^*}{g_\theta + g_\theta^*}\right)^2 \text{Im} d_2(M_{1,1}^2)}{\left(g_\theta + g_\theta^* - \frac{4g_\theta g_\theta^*}{g_\theta + g_\theta^*}\right)^2 (\text{Im} d_2(M_{1,1}^2))^2}$$

$$= 4 \quad (206)$$

and, therefore, the same resonance height as for the first parity allowed resonance in the $\theta = 0$ case (200).

At the parity forbidden threshold $s = (M_2 + \mu)^2$, where $\text{Im} d_{1,1}((M_2 + \mu)^2)$ is singular, we find

$$\sigma_{2\mu \rightarrow f}^{\text{tot}}((M_2 + \mu)^2) \simeq \frac{r_1^2}{w((M_2 + \mu)^2, \mu^2, \mu^2)}.$$

$$\begin{aligned}
& \cdot \text{Im} \frac{g_\theta + g_\theta^* - 4ig_\theta g_\theta^* \text{Im} d_{1,1}((M_2 + \mu)^2)}{1 - i(g_\theta + g_\theta^*)(\text{Im} d_2 + \text{Im} d_{1,1}) - 4g_\theta g_\theta^* \text{Im} d_2 \text{Im} d_{1,1}} = \\
& \frac{r_1^2}{w((M_2 + \mu)^2, \mu^2, \mu^2)} \frac{(g_\theta + g_\theta^*)^2 (\text{Im} d_2 + \text{Im} d_{1,1}) - 4g_\theta g_\theta^* \text{Im} d_{1,1} (1 - 4g_\theta g_\theta^* \text{Im} d_2 \text{Im} d_{1,1})}{(1 - 4g_\theta g_\theta^* \text{Im} d_2 \text{Im} d_{1,1})^2 + (g_\theta + g_\theta^*)^2 (\text{Im} d_2 + \text{Im} d_{1,1})^2} \\
& \rightarrow \frac{r_1^2}{w((M_2 + \mu)^2, \mu^2, \mu^2)} \frac{4g_\theta g_\theta^* (\text{Im} d_{1,1})^2 \text{Im} d_2}{(g_\theta + g_\theta^*)^2 (\text{Im} d_{1,1})^2} \rightarrow \left(\frac{4g_\theta g_\theta^*}{g_\theta + g_\theta^*} \right)^2 \frac{r_1^2 \text{Im} d_2 ((M_2 + \mu)^2)}{w((M_2 + \mu)^2, \mu^2, \mu^2)}
\end{aligned} \tag{207}$$

where we performed the limit $\text{Im} d_{1,1} \rightarrow \infty$ and kept only the lowest order contribution in g_θ . Therefore, in contrast to the parity allowed case, the parity forbidden thresholds do not give zero in σ^{tot} .

The reason for this behaviour may be easily understood. In the limit of $\theta \rightarrow 0$ there should not remain any effect of resonances or thresholds in σ^{tot} for parity forbidden transitions, and σ^{tot} should be described by the lowest order result (190).

Precisely this happens: Although the resonance height at $M_{1,1}^2$ remains unchanged for $\theta \rightarrow 0$, (206), its width tends to zero, (181). This means that the resonance $M_{1,1}$ still exists but is stable against $M_{1,1} \rightarrow 2\mu$ decay for $\theta \rightarrow 0$. Actually the $M_{1,1}$ bound state is a stable particle at all for $\theta = 0$. Further, at threshold $s = (M_2 + \mu)^2$, σ^{tot} tends to the first order result (190) for $\theta \rightarrow 0$,

$$\lim_{\theta \rightarrow 0} \left(\frac{4g_\theta g_\theta^*}{g_\theta + g_\theta^*} \right)^2 = m^2 \Sigma^2 + o(m^3) \tag{208}$$

as it should hold.

For even higher s , when both parity allowed and parity forbidden final states are possible, we again have the problem that the relative sign of the parity forbidden process is "wrong" due to our conventions (see the remark after equ. (169)). E.g. at the M_3 resonance we find from (203)

$$\begin{aligned}
\sigma_{2\mu \rightarrow f}^{\text{tot}}(s = M_3^2) & \simeq \frac{r_1^2}{w(M_3^2, \mu^2, \mu^2)} \cdot \\
& \text{Im} \frac{g_\theta + g_\theta^* - 4g_\theta g_\theta^* \text{Re} d_3(M_3^2)}{-i(g_\theta + g_\theta^*)(\text{Im} d_2(M_3^2) + \text{Im} d_{1,1}(M_3^2)) + 4ig_\theta g_\theta^* \text{Re} d_3(M_3^2) \text{Im} d_2(M_3^2)} \\
& = \frac{r_1^2}{w(M_3^2, \mu^2, \mu^2)} \frac{g_\theta + g_\theta^* - \frac{4g_\theta g_\theta^*}{g_\theta + g_\theta^*}}{(g_\theta + g_\theta^* - \frac{4g_\theta g_\theta^*}{g_\theta + g_\theta^*}) \text{Im} d_2(M_3^2) + (g_\theta + g_\theta^*) \text{Im} d_{1,1}(M_3^2)} \\
& \simeq \frac{r_1^2}{w(M_3^2, \mu^2, \mu^2)} \frac{m\Sigma(\cos \theta - \frac{1}{\cos \theta})}{m\Sigma(\cos \theta - \frac{1}{\cos \theta}) \text{Im} d_2(M_3^2) + m\Sigma \cos \theta \text{Im} d_{1,1}(M_3^2)} \\
& \rightarrow \frac{r_1^2}{w(M_3^2, \mu^2, \mu^2)} \frac{\frac{1}{\cos \theta} - \cos \theta}{(\frac{1}{\cos \theta} - \cos \theta) \text{Im} d_2(M_3^2) + \cos \theta \text{Im} d_{1,1}(M_3^2)} \\
& = \frac{r_1^2}{w(M_3^2, \mu^2, \mu^2)} \frac{\sin^2 \theta (\sin^2 \theta \text{Im} d_2(M_3^2) + \cos^2 \theta \text{Im} d_{1,1}(M_3^2))}{[\sin^2 \theta \text{Im} d_2(M_3^2) + \cos^2 \theta \text{Im} d_{1,1}(M_3^2)]^2}
\end{aligned} \tag{209}$$

where the last two lines are for real θ (the last line may be easily checked by a low order reasoning, in case somebody does not trust our imaginary θ convention).

Again, the resonance height (containing two partial decay channels) does not depend on the coupling constant.

For even higher s the above pattern repeats.

The last thing to be discussed is the contribution of the t and u channel diagrams. There the lowest order diagram must be subtracted (see Fig. 14),

$$\mathcal{M}'_{2\mu \rightarrow 2\mu}(t) = S^T \mathcal{G}(\Pi(t) - 1) S \quad (210)$$

where $t = 4\mu^2 - s \leq 0$, $u \equiv 0$.

It is a wellknown fact that the t and u channel amplitudes in the case at hand have no singularities on the physical sheet of the complex s plane, and, therefore, no imaginary parts (see e.g. [65]). They are, themselves, imaginary parts of some higher order graphs (in fact, of the non-factorizable four-point function of Fig. 14). As a consequence, the $\mathcal{M}'(t)$, $\mathcal{M}'(u = 0)$ contributions are small for all t and cannot change the above-discussed behaviour. The only point where $\mathcal{M}'(t)$, $\mathcal{M}'(u)$ cause a qualitative change is the elastic threshold $s = 4\mu^2$, $t = 0$. There the lowest order singular behaviour, equ. (190), that was cancelled by the s -channel contribution, equ. (205), is retained, but with a different coefficient. We find indeed

$$\begin{aligned} \sigma_{2\mu \rightarrow 2\mu}(s \sim 4\mu^2) &= \frac{r_1^4}{w^2(s \sim 4\mu^2, \mu^2, \mu^2)} |\mathcal{M}_{2\mu \rightarrow 2\mu}(s \sim 4\mu^2) + 2\mathcal{M}'_{2\mu \rightarrow 2\mu}(0)|^2 \\ &\simeq \frac{r_1^4}{w^2(s \sim 4\mu^2, \mu^2, \mu^2)} |2\mathcal{M}'_{2\mu \rightarrow 2\mu}(0)|^2 \\ &\simeq \frac{r_1^4}{w^2(s \sim 4\mu^2, \mu^2, \mu^2)} 4 \left(\frac{2g_\theta g_\theta^* \tilde{E}_-(0) + (g_\theta^2 + g_\theta^{*2}) \tilde{E}_+(0)}{1 - (g_\theta + g_\theta^*) \tilde{E}_+(0)} \right)^2 \\ &\rightarrow \infty \quad \text{for} \quad s \rightarrow 4\mu^2 \end{aligned} \quad (211)$$

where $\mathcal{M}_{2\mu \rightarrow 2\mu}(4\mu^2)$ is given by (193) (including the lowest order), and $\mathcal{M}'_{2\mu \rightarrow 2\mu}(0)$ is given by (210) (without lowest order). The $\tilde{E}_\pm(0)$ are just the E_\pm of Section 5 (see (64), (67)).

Further, whenever the s -channel cross section vanishes (at parity allowed higher production thresholds), its value is changed from zero to a small nonzero number (of order $(m\Sigma)^4$).

All the other features of the s -channel scattering cross section remain unchanged.

XII. SUMMARY

It is our hope that the discussion of the previous sections has convinced the reader that the massive Schwinger model exhibits quite a rich quantum-field theoretic structure and, therefore, is worth studying.

The mass perturbation theory – which was the basic ingredient of our approach – is similar to the derivation of a low-energy effective theory in realistic models like QCD. In our approach only bosonic states (fermion-antifermion bound states) are present as physical states. The (dimensionfull) coupling constant e plays a role similar to Λ_{QCD} within our

model. In fact, because of the small number of degrees of freedom ($N_f = 1$) this model mimicks, up to a certain extent, the η' dynamics of QCD.

A further advantage of the mass perturbation expansion is the fact that – in contrast to ordinary perturbation theory – nontrivial phenomena, like instanton vacuum and fermion condensates, may be discussed quite straight forwardly (actually, all the computations throughout the article are for general vacuum angle θ).

A first major point in the discussion of the model was the computation of the vacuum functional and vacuum energy density. As a consequence, the mass perturbation theory could be shown to be IR-finite.

After deriving the matrix-valued Feynman rules of the mass perturbation theory, we could actually give quite a complete description of the physical properties of the model. We were able to compute the condensates and susceptibilities and to give an exact description of the confinement behaviour.

Further we succeeded in performing a resummation of the perturbation series for the n -point functions with the help of the Dyson-Schwinger equations. These resummed n -point functions turned out to be very useful for a further discussion of the physical properties of the model. We could infer the whole spectrum of (stable) particles and (unstable) bound states from the two-point function. Further we were able to identify all the partial decay channels of all bound states. As an illustration, we computed some bound-state masses and decay widths.

At last we discussed scattering processes and found that all the unstable bound states turn into resonances of the scattering cross section, as has to be expected. Further, with the help of unitarity we were able to identify all the possible final states that may exist for the scattering of a given initial state.

As a result, the following physical picture emerged: there exist two stable particles in the theory, namely the Schwinger boson μ and the two-boson bound state M_2 . Higher (unstable) bound states may be formed out of an arbitrary number of μ and M_2 . Further, these unstable bound states may decay into all combinations of μ and M_2 that are possible kinematically. (For the special case $\theta = 0$ the lowest mixed bound state, composed of one μ and one M_2 , is stable, too, because of parity conservation, and is therefore present both in final and intermediate states, analogous to our discussion of the M_2 particle; however, we treated the generic $\theta \neq 0$ case throughout the article and, therefore, did not discuss this straight-forward generalization in detail.)

For scattering processes we found that far from all resonances and particle production thresholds the scattering cross section is well described by a lowest order computation. Whenever the squared momentum s is near a bound-state mass, the scattering cross section has a local maximum, i.e. a resonance occurs. Moreover, for all values of s where a new final state becomes possible kinematically, the corresponding real particle production threshold indeed occurs.

We want to emphasize that all these features result from our resummed mass perturbation theory, and that we did not have to impose further assumptions or use further approximations in order to find this physical structure.

There are (at least) two directions of further study within this field that we believe to be important. On one hand, an increase of the number of fermions ($N_f > 1$) further enriches the complexity of the model and makes it possible to mimick the light field dynamics (pions)

of QCD, too. There exists some work on the massive multi-flavour Schwinger model that uses bosonization and/or semiclassical methods ([25,33,21,60,61,59]). It would be very interesting to discuss this model analogously to our discussion in the previous sections; however, a direct application of the mass perturbation expansion is not possible there, because it fails to be IR-convergent [33]. Therefore, more elaborate methods should be developed for a further study.

On the other hand, the properties we found hold for sufficiently small fermion mass m (strong coupling e). Of course, it would be interesting to understand whether and how the physical structure of the model changes when the fermion mass is increased. Perhaps a discussion similar to this article for the massive Schwinger model within ordinary (electrical charge) perturbation theory and a comparison of the two approaches could be a first step towards getting more insight into this question.

In any case, QED₂ remains a fascinating subject of study that will offer further insight into general concepts of quantum field theory as well as into some deep problems of QCD.

ACKNOWLEDGEMENT

The author thanks R. Jackiw for the opportunity to join the Center of Theoretical Physics at MIT, where this work was finished, and the CTP members for their hospitality. Further, this work has greatly benefitted from discussions with various scientists. The author owes special thanks to C. Gattringer, H. Grosse, M. Hutter, R. Jackiw, H. Leutwyler, J. Pawłowski, A. V. Smilga and A. Wipf.

This work is supported by a Schrödinger stipendium of the Austrian FWF.

REFERENCES

- [1] J. Schwinger, *Phys. Rev.* **128** (1962), 2425.
- [2] J. Lowenstein, J. Swieca, *Ann. Phys.* **68** (1971), 172.
- [3] C. Jayewardena, *Helv. Phys. Acta* **61** (1988), 636.
- [4] I. Sachs, A. Wipf, *Helv. Phys. Acta* **65** (1992), 653.
- [5] I. Sachs, A. Wipf, *Ann. Phys.* **249** (1996), 380.
- [6] A. Dettki, I. Sachs, A. Wipf, preprint ETH-TH/93-14.
- [7] W. Dittrich, M. Reuter, "Selected topics ...", *Lecture Notes in Physics* **244**, Springer Verlag, Berlin 1986.
- [8] Y. Frishman, *Lecture Notes in Physics* **32**, Springer Verlag, Berlin 1975.
- [9] H. Grosse, "Models in statistical physics and quantum field theory", Springer Verlag, Berlin 1988.
- [10] R. E. Gamboa Saravi, M. A. Muschietti, F. A. Schaposnik, J. E. Solomin, *Ann. Phys.* **157** (1984), 360.
- [11] E. Abdalla, M. Abdalla, K. D. Rothe, "2 dimensional Quantum Field Theory", World Scientific, Singapore 1991.
- [12] R. Jackiw, "Topological investigations ...", in: Treiman et al, "Current algebras and anomalies", World Scientific, Singapore 1985.
- [13] R. A. Bertlmann, "Anomalies in quantum field theory", Clarendon Press, Oxford 1996.
- [14] N. P. Ilieva, V. N. Pervushin, *Sov. J. Part. Nucl.* **22** (1991), 275.
- [15] A. Casher, J. Kogut, P. Susskind, *Phys. Rev.* **D10** (1974), 732.
- [16] J. Kogut, P. Susskind, *Phys. Rev.* **D11** (1975), 3594.
- [17] C. Adam, R. A. Bertlmann, P. Hofer, *Riv. Nuovo Cim.* **16** (1993), 1.
- [18] C. Adam, *Z. Phys.* **C63** (1994), 169.
- [19] C. Adam, thesis, Universität Wien 1993.
- [20] C. Adam, *Czech. J. Phys.* **46** (1996), 893, hep-ph 9501273.
- [21] A. V. Smilga, *Phys. Lett.* **B278** (1992), 371.
- [22] A. V. Smilga, *Phys. Rev.* **D46** (1992), 5598.
- [23] A. V. Smilga, *Phys. Rev.* **D49** (1994), 5480.
- [24] S. Coleman, R. Jackiw, L. Susskind, *Ann. Phys.* **93** (1975), 267.
- [25] S. Coleman, *Ann. Phys.* **101** (1976), 239.
- [26] M. P. Fry, *Phys. Rev.* **D47** (1993), 2629.
- [27] C. Adam, *Phys. Lett.* **B 363** (1995), 79, hep-ph 9507279.
- [28] C. Adam, *Phys. Lett.* **B 382** (1996), 383, hep-ph 9507331.
- [29] J. Fröhlich, *Comm. Math. Phys.* **47** (1976), 233.
- [30] J. Fröhlich, E. Seiler, *Helv. Phys. Acta* **49** (1976), 889.
- [31] J. Steele, A. Subramanian, I. Zahed, *Nucl. Phys.* **B452** (1995), 545, hep-th 9503220.
- [32] C. Gattringer, E. Seiler, *Ann. Phys.* **233** (1994), 97.
- [33] C. Gattringer, hep-th 9503137; *Ann. Phys.* **250** (1996), 389, hep-th 9602027.
- [34] C. Adam, preprint PM 96/01, hep-ph 9601227.
- [35] C. Adam, *Phys. Lett.* **B 382** (1996), 111, hep-th 9602175.
- [36] N. K. Nielsen, B. Schroer, *Nucl. Phys.* **B120** (1977), 62.
- [37] N. K. Nielsen, B. Schroer, *Nucl. Phys.* **B127** (1977), 493.
- [38] H. J. Rothe, K. D. Rothe, J. A. Swieca, *Phys. Rev.* **D19** (1979), 3020.
- [39] M. Hortacsu, K. D. Rothe, B. Schroer, *Phys. Rev.* **D20** (1979), 3203.

- [40] K. D. Rothe, B. Schroer, *Nucl. Phys.* **B185** (1981), 429; **B172** (1980), 383.
- [41] R. Baier, E. Pilon, *Z. Phys.* **C52** (1991), 339.
- [42] H. Leutwyler, A. V. Smilga, *Phys. Rev.* **D46** (1992), 5607.
- [43] A. V. Smilga, J. J. M. Verbaarschot, *Phys. Rev.* **D54** (1996), 1087, hep-ph 9511471.
- [44] D. J. Gross, I. R. Klebanov, A. V. Matytsin, A. V. Smilga, *Nucl. Phys.* **B461** (1996), 109, hep-th 9511104.
- [45] E. Abdalla, R. Mohayaee, A. Zadra, hep-th 9604063.
- [46] J. P. Vary, T. J. Fields, H. J. Pirner, *Phys. Rev.* **D53** (1996), 7231, hep-ph 9411263.
- [47] K. Harada et al, *Phys. Rev.* **D52** (1995), 2492, hep-th 9509136.
- [48] T. Eller, H. C. Pauli, S. J. Brodsky, *Phys. Rev.* **D35** (1987), 1493.
- [49] T. Eller, H. C. Pauli, *Z. Phys.* **C42** (1989), 59.
- [50] S. Elser, H. C. Pauli, A. C. Kallionatis, hep-th 9505069.
- [51] S. Elser, A. C. Kallionatis, hep-th 9601045.
- [52] D. P. Crewther, C. J. Hamer, *Nucl. Phys.* **B170** (1980), 353.
- [53] C. J. Hamer et al, *Nuc. Phys.* **B208** (1982), 413.
- [54] S. R. Carson, R. D. Kenway, *Ann. Phys.* **166** (1986), 364.
- [55] H. Gausterer, C. B. Lang, *Phys. Lett.* **B341** (1994), 46.
- [56] H. Gausterer, C. B. Lang, *Nucl.Phys.* **B455** (1995), 785.
- [57] C. Gatttringer, *Phys. Rev.* **D53** (1996), 5090.
- [58] R. D. Peccei, H. R. Quinn, *Phys. Rev.* **D16** (1977), 1791; *Phys. Rev. Lett.* **38** (1977), 1440.
- [59] M. Sadzikowski, P. Wegrzyn, hep-ph 9605242.
- [60] M. Paranjape, *Phys. Rev.* **D48** (1993), 3892; 4946.
- [61] J. E. Hetrick, Y. Hosotani, S. Ito, hep-th 9502113.
- [62] C. Adam, *Phys. Lett.* **B391** (1997), 395, hep-th 9609154.
- [63] C. Adam, preprint FSUJ-TPI-16/96, hep-th 9610050.
- [64] C. Adam, preprint MIT-CTP-2602 (1997), hep-th 9701013.
- [65] R. J. Eden, P. V. Landshoff, D. I. Olive, J. C. Polkinghorne, “The Analytic S -Matrix”, Cambridge University Press, Cambridge 1966.